Mean and Variability of the WHOI Daily Latent and Sensible Heat Fluxes at In Situ Flux Measurement Sites in the Atlantic Ocean*

LISAN YU, ROBERT A. WELLER, AND BOMIN SUN+

Department of Physical Oceanography, Woods Hole Oceanographic Institution, Woods Hole, Massachusetts

(Manuscript received 2 July 2003, in final form 16 December 2003)

ABSTRACT

Daily latent and sensible heat fluxes for the Atlantic Ocean from 1988 to 1999 with 1° × 1° resolution have been recently developed at Woods Hole Oceanographic Institution (WHOI) by using a variational object analysis approach. The present study evaluated the degree of improvement made by the WHOI analysis using in situ buoy/ship measurements as verification data. The measurements were taken from the following field experiments: the five-buoy Subduction Experiment in the eastern subtropical North Atlantic, three coastal field programs in the western Atlantic, two winter cruises by R/V *Knorr* from the Labrador Sea Deep Convection Experiment, and the Pilot Research Moored Array in the Tropical Atlantic (PIRATA). The differences between the observed and the WHOI-analyzed fluxes and surface meteorological variables were quantified. Comparisons with the outputs from two numerical weather prediction (NWP) models were also conducted.

The mean and daily variability of the latent and sensible heat fluxes from the WHOI analysis are an improvement over the NWP fluxes at all of the measurement sites. The improved flux representation is due to the use of not only a better flux algorithm but also the improved estimates for flux-related variables. The mean differences from the observations in latent heat flux and sensible heat flux, respectively, range from 2.9 (3% of the corresponding mean measurement value) and 1.0 W m^{-2} (13%) at the Subduction Experiment site, to 11.9 (13%) and 0.7 W m^{-2} (11%) across the PIRATA array, to 15.9 (20%) and 10.5 W m^{-2} (34%) at the coastal buoy sites, to 8.7 (7%) and 9.7 W m^{-2} (6%) along the *Knorr* cruise tracks. The study also suggests that further improvement in the accuracy of latent and sensible heat fluxes will depend on the availability of high-quality SST observations and improved representation/observations of air humidity in the tropical Atlantic.

1. Introduction

Daily latent and sensible heat flux fields for the Atlantic Ocean (65°S–65°N) from 1988 to 1999 with 1° × 1° resolution have been recently developed at the Woods Hole Oceanographic Institution (WHOI; Yu et al. 2004). The development was based on the following two procedures: First, the estimates of the flux-related surface meteorological variables (i.e., wind speed, specific air humidity, air temperature, and sea surface temperature) were obtained from a synthesis process using a variational objective analysis. The input data for the synthesis included satellite retrievals and also outputs from two numerical weather prediction (NWP) models, that is, the European Centre for Medium-Range Weather Forecasts (ECMWF) operational forecast model and the National Centers for Environmental Prediction version 2 (NCEP2) reanalysis forecast model (Kalnay et al. 1996; Kanamitsu et al. 2000). Second, the flux-related variables determined from the synthesis were applied to the Tropical Ocean and Global Atmosphere Coupled Ocean–Atmosphere Response Experiment (TOGA COARE) bulk flux algorithm 2.6a (Fairall et al. 1996; Bradley et al. 2000) to compute the latent and sensible heat fluxes. Since the synthesis produces an optimal estimate that has minimum error variance (Daley 1991) and the COARE flux algorithm 2.6a represents a state-of-the-art bulk flux parameterization (Zeng et al. 1998), it is anticipated that the WHOI turbulent heat flux fields would be an improvement. The present study assesses the degree of improvement that was achieved by using in situ buoy/ship flux measurements as verification data.

Accurate representation of turbulent latent and sensible heat exchanges at the air–sea interface is of great interest to the climate research community for studying coupled variability of the atmosphere–ocean system. Two common types of errors can affect the accuracy of a flux product: systematic errors that bias the mean and random errors that influence the variance. Therefore, the mean and variability of the flux field are the two features

* Woods Hole Oceanographic Institution Contribution Number 10972.

+ Current affiliation: NOAA/National Climate Data Center, Asheville, North Carolina.

Corresponding author address: Dr. Lisan Yu, Department of Physical Oceanography, Woods Hole Oceanographic Institution, MS #21, Woods Hole, MA 02543.
E-mail: lyu@whoi.edu

at the heart of the assessment. To do so, two existing datasets are used. One is the flux climatology analysis that was composed from marine surface weather reports from the Voluntary Observing Ships program. These flux climatologies provide the first-order depiction of global air–sea heat exchanges on a climatological mean basis, but differences do exist between different climatologies due to the use of different methodologies, different bulk algorithms, and different data processing/smoothing procedures (Gleckler and Weare 1997). Because of the large uncertainties, the flux climatologies can serve as a reference but not as the verification data. The other dataset is in situ buoy/ship flux measurements at limited locations. Those observations have high accuracy and have been used as benchmark time series for quantification of regional biases in NWP model outputs (Weller and Anderson 1996; Moyer and Weller 1997; Weller et al. 1998; Josey 2001; Smith et al. 2001; Wang and McPhaden 2001; Renfrew et al. 2002; Sun et al. 2003). A number of the buoys that were equipped with two redundant sensor sets and the time series that were also not assimilated by the NWP models are of particular value for verification. These buoys are referred to as flux buoys. Over the 12-yr synthesis period from 1988 to 1999, there exist a dozen flux buoy deployments plus the Pilot Research Moored Array in the Tropical Atlantic (PIRATA) array and a few cruises in the Atlantic basin (Fig. 1). All of them are located north of 15°S.

The comparison of the long-term mean aspect of the WHOI fluxes with the flux climatology analysis of the Southampton Oceanographic Centre (SOC; Josey et al. 1998, 1999) as the reference was conducted in a previous study (Yu et al. 2004). That study showed that the mean field structure and year-to-year variations of the WHOI latent and sensible heat fluxes are in good agreement with those of the SOC fluxes, despite different data sources and different temporal resolutions used in constructing the two products. That study also indicated that the WHOI fluxes are different from the ECMWF and NCEP2 flux outputs and that the differences come not only from the use of a better flux algorithm but also from the use of the improved estimates of bulk variables. Yet, accurate quantification of the WHOI flux analysis can only be obtained using high-accuracy in situ flux measurements—a focal issue to be addressed in the present study. In a sense, this paper represents a continuation of our evaluation efforts. On a broader aspect, these efforts result from our ongoing project of developing high-quality, gridded, time-dependent surface turbulent and radiative fluxes to support studies of the Atlantic climate variability and predictability under the auspices of the National Oceanic and

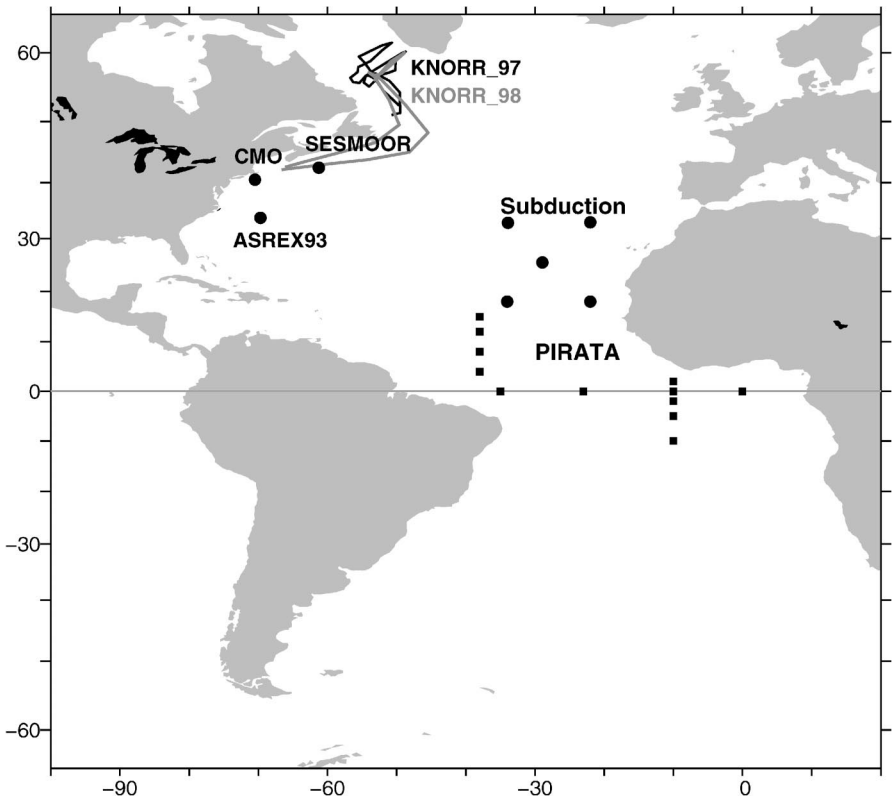

FIG. 1. Location of flux buoys and ship tracks used in the validation.

Atmospheric Administration (NOAA) Climate Variability and Predictability (CLIVAR) Atlantic program.

The presentation is organized in the following way. Section 2 provides a brief overview of the daily latent and sensible heat fluxes produced from the WHOI synthesis. Section 3 describes the processing procedure and the basic characteristics of in situ measurements. Section 4 evaluates the mean and variability of the daily flux product at in situ measurement sites. Section 5 presents discussions of two issues, the influence of satellite observations on the estimation of flux-related basic variables and the improvement over the ECMWF and NCEP2 basic variables and fluxes. Summary and conclusions are included in section 6.

2. The latent and sensible heat fluxes estimated from the WHOI analysis

a. Overview of the WHOI flux analysis

The WHOI daily latent and sensible heat fluxes for the Atlantic Ocean extend from 65°S to 65°N and cover the period from 1988 to 1999 with $1° \times 1°$ resolution. The fluxes were computed from the COARE algorithm 2.6a using basic surface meteorological variables determined from a variational objective analysis. Several data sources were synthesized in the objective analysis, including wind speed (Wentz 1997) and air specific humidity (Chou et al. 2003) from the Special Sensor Microwave Imager (SSM/I), sea surface temperature (SST) from the Advanced Very High Resolution Radiometer (AVHRR), and the surface meteorological variables from the ECMWF operational forecast model and the NCEP2 reanalysis forecast model.

The variational objective analysis involves a direct minimization of an objective function that consists of a number of terms, each measuring the departure of the analysis field from input data fields. Associated with each term is a weight that is inversely proportional to the error covariance of input data. A conjugate-gradient method is employed iteratively to find the optimal solution of the objective function. Daily estimates of basic variables at the optimal solution are then used together with the COARE algorithm 2.6a to compute daily latent and sensible heat fluxes. Readers are referred to Yu et al. (2002, 2004) for detailed discussions on the methodology of the objective analysis, the approach used to compute error variances (weights) for input data, and the sensitivity of the solution field to weight assignments.

In the following analysis, only the flux fields north of 25°S are shown, as there are no in situ flux measurements existing south of this latitude.

b. Seasonal variations of latent and sensible heat flux fields

The fields of latent (Q_{LH}) and sensible (Q_{SH}) heat fluxes in January and July averaged over the synthesis period from 1988 to 1999 are plotted in Fig. 2. Negative fluxes indicate heat loss from the ocean, while positive fluxes indicate heat gain by the ocean. Both latent and sensible heat flux fields exhibit strong seasonal variations, particularly at high latitudes and near the western boundary. For instance, the oceanic latent heat loss over the Gulf Stream is of order -225 W m^{-2} in January but is only about -75 W m^{-2} in July. The sensible heat flux in the Labrador Sea changes from a large amount of heat loss (~ -100 W m^{-2}) in January to a small amount of heat gain (~ 10 W m^{-2}) in July. Away from the western boundary, seasonal variations are small in the sensible heat flux fields but still quite significant in the latent heat flux fields. In the latter, pronounced seasonality is most evident in two regions: the subtropics and the equatorial cold tongue where the intensity of latent heat loss is stronger in winter and weaker in summer.

3. Description of in situ flux measurements

a. Overview of in situ measurements

The verification time series (Fig. 1) are chosen from the following field experiments: the Subduction Experiment in the eastern subtropical North Atlantic that consisted of five buoys (Moyer and Weller 1997), three coastal field programs in the western North Atlantic named the Severe Environment Surface Mooring (SESMOOR; Crescenti et al. 1991), the Coastal Mixing and Optics Experiment (CMO; Galbraith et al. 1999), and the 1993 Acoustic Surface Reverberation Experiment (ASREX93; Galbraith et al. 1996), the Labrador Sea Deep Convection Experiment that resulted in two winter cruises (Bumke et al. 2002), and the Pilot Research Moored Array in the Tropical Atlantic (PIRATA; Servain et al. 1998) that has 11 buoys operating since 1997. The location, period, and instrument types of the experiments are summarized in Table 1.

Subduction Experiment, CMO, SESMOOR, and ASREX93 used WHOI instrumentation that measures surface pressure, ocean surface temperature at 1-m depth, relative humidity and air temperature at $\sim$2.7-m height, and wind speed and direction at $\sim$3.4-m height (Weller and Anderson 1996). The data were averaged over 15-min intervals during postprocessing (Moyer and Weller 1997). The PIRATA array carries Autonomous Temperature Line Acquisition System (ATLAS) buoys that collect 10-min-averaged ocean surface temperature at 1-m depth, relative humidity and air temperature at 3-m height, and wind speed and direction at 4-m height. The observing system on board R/V *Knorr* was the Improved Meteorological package (IMET) that samples ocean surface temperature at 2 m below the surface and all other surface meteorological quantities at 23-m height and provides 5-min averages (Renfrew et al. 2002). All the buoy/ship data, except for wind and air temperature observations from PIRATA, were withheld

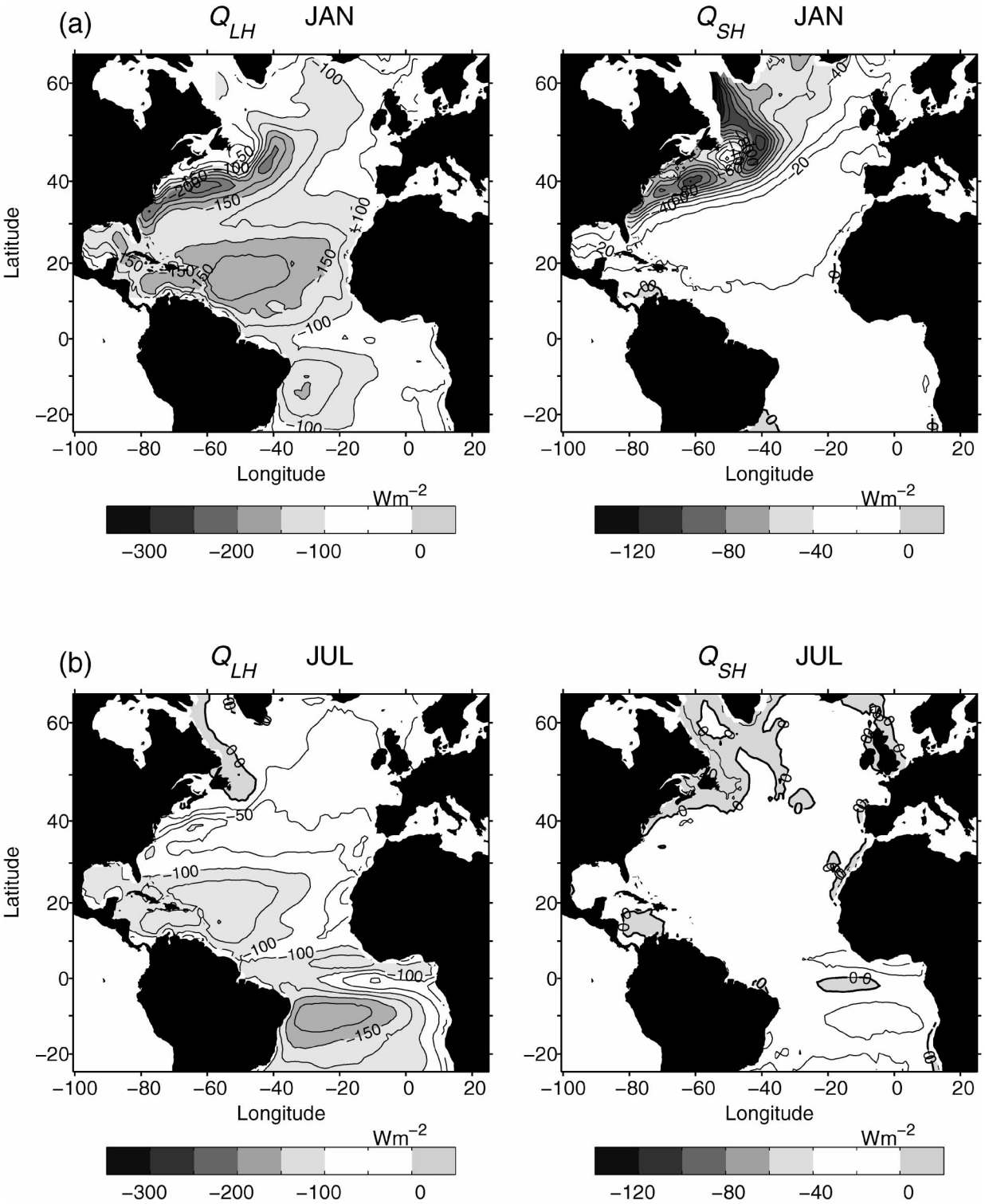

FIG. 2. Seasonal variations of latent and sensible heat fluxes in the Atlantic Ocean in (a) Jan and (b) Jul. Contour interval is 25 W m^{-2} for the latent heat flux (Q_{LH}) field and 10 W m^{-2} for the sensible heat flux (Q_{SH}) field. The seasonal data are constructed for the period from 1988 to 1999.

TABLE 1. List of the flux measurements used in the validation.

Expt	Location	Deployment period	Measurement instruments
Subduction (5-buoy array)	Eastern North Atlantic [18°–33°N, 22°–34°W]	Jun 1991–Jun 1993	WHOI Improved Meterological Recorder (IMET)
Coastal region (3 buoys)	Western North Atlantic		
CMO	[40.5°N, 70.5°W]	Aug 1996–Jun 1997	WHOI instruments
SESMOOR	[42.6°N, 61.2°W]	Oct 1988–Mar 1989	
ASREX	[33.9°N, 69.8°W]	Dec 1993–Mar 1994	
PIRATA (12-buoy array)*	Tropical Atlantic [5°S–10°N, 38°W–0°]	Start dates vary, but all between 1997 and 2000	ATLAS
Labrador Sea Deep Convection (2 *Knorr* cruises)	Labrador Sea [48°–62°N, 58°–46°W]	5 Feb–13 Mar 1997 20 Jan–13 Feb 1998	*Knorr*'s Improved Meterological package (IMET)

* The buoy at 3.5°N, 38°W is not used because only a few days of the data are available for our synthesis period 1988–99.

from being assimilated by the NWP centers so that they would be independent of the model fields.

To facilitate the comparison, buoy/ship measurements were processed in a way similar to our previous study (Sun et al. 2003). In particular, air specific humidity was derived from relative humidity and air temperature using the TeTen formula (Bolton 1980). The measured wind speed was height adjusted to the 10-m reference height and air temperature and humidity were adjusted to the 2-m reference height by using the COARE 2.6a algorithm (Bradley et al. 2000). The measurements were daily averaged and applied to the COARE 2.6a bulk formulas to produce daily latent and sensible heat fluxes. To obtain the WHOI analysis values at the buoy sites and along the ship tracks, a bilinear interpolation was applied using the analysis values at the surrounding four grid points. Special attention is paid to the three buoys in the coastal regions of the western North Atlantic where the surface fields change dramatically across the Gulf Stream front. For those cases, only the values at the analysis grid points that most closely replicate the buoy observations were considered in the interpolation. The same interpolation procedure was applied when extracting the ECMWF and NCEP values at the measurement sites.

b. Characteristics of the regional climate at the measurement sites

As the latent and sensible heat fluxes are predominantly determined by a combination of wind speed and sea–air humidity/temperature gradients, changes in the atmospheric and oceanic circulation give rise to changes in the fluxes. To gain a better understanding of the variability of the time series recorded by in situ instruments, a brief overview of major meteorological and oceanic conditions surrounding the buoy/ship locations is provided. The monthly mean sea level pressure (SLP) and SST fields in January and July from the SOC climatology analysis (Josey et al. 1998) are shown in Fig. 3 with the buoy locations and ship tracks superimposed. The fields represent the averages over the period from 1988 to 1997. The mean atmospheric circulation in the North Atlantic is largely governed by two pressure centers: the Icelandic low located at the southern tip of Greenland north of 50°N, and the Azores high centered at 30°N in the subtropics. Major characteristics of seasonal climate variations at in situ measurement sites are summarized in the following:

- The climate in the eastern subtropical North Atlantic where the five-buoy subduction array was located is under the influence of the Azores high pressure system all year-round (Moyer and Weller 1997). The region features northeasterly trade winds and moderate seasonal SST changes.
- The climate in the midlatitude western Atlantic where the three coastal field programs (CMO, SESMOOR, and ASREX) were conducted was influenced by the Gulf Stream, its variations, and synoptic weather systems. The three buoys were all deployed between the months of October and May, though in different years (Table 1). The sites of the CMO (40.5°N, 70.5°W) and SESMOOR (42.6°N, 61.2°W) buoys are adjacent north of the Gulf Stream, surrounded by a strong meridional SST gradient (Figs. 3c,d). During wintertime, the region is susceptible to synoptic weather events that bring cold, dry continental air to the relatively warm moist sea surface and produce very high rates of latent and sensible heat loss from the ocean (e.g., Bane and Osgood 1989; Crescenti and Weller 1992). The SESMOOR experiment was designed to document air–sea interactions during rapidly intensifying winter cyclones (Crescenti et al. 1991), so the buoy was deployed in the neighborhood of maximum cyclone occurrence (Roebber 1984). In comparison, the environment at the ASREX buoy site (34°N, 70°W) is different. The site is located to the south of the Gulf Stream, away from SST gradients. In addition, this site is on the western edge of the Azores high and typically sees southeasterly winds year-round. There can be a cold weather system passing through from

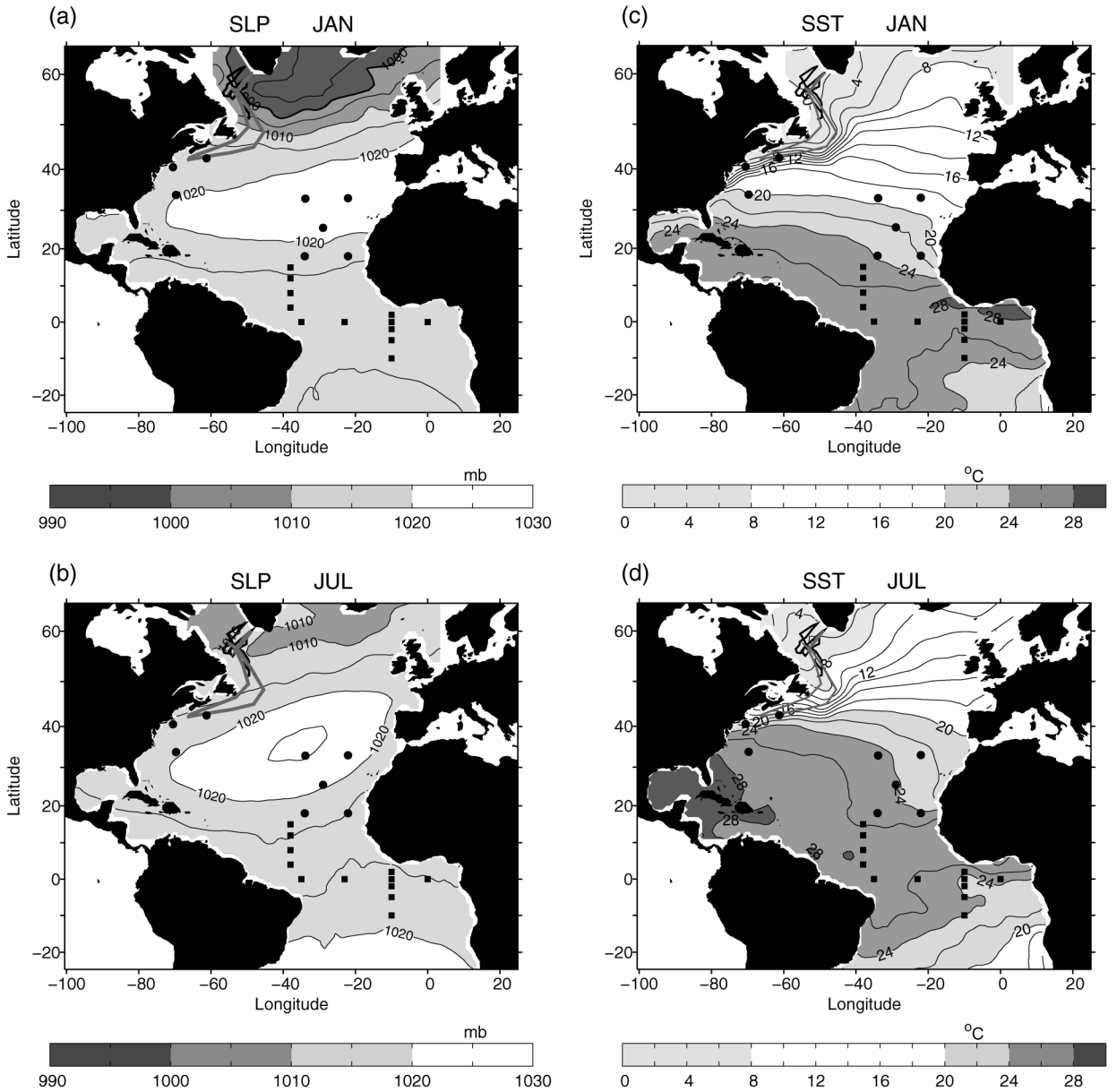

FIG. 3. As in Fig. 2 but for the SLP field in (a) Jan and (b) Jul, and for the SST field in (c) Jan and (d) Jul. Contour interval is 5 mb for the SLP field and 2°C for the SST field.

the northwest continent but not so frequently as at the SESMOOR site.

- The Labrador Sea in winter is governed by the Icelandic low pressure system and is subject to northwesterly winds that carry cold and dry air masses from continents to the north and west. These air masses contrast sharply with the relatively warm, moist surface of the ice-free sea, which, along with strong winds, can lead to extremely high losses of latent and sensible heat from the ocean (Marshall et al. 1998). The two *Knorr* cruises in the winters of 1997 and 1998 (Table 1) documented some of the most intensive sea surface cooling events ever directly observed.
- The 12-buoy PIRATA array extends over the tropical Atlantic sector and embraces the northeast and southeast trades, the intertropical convergence zone, the warm pool, and cold tongue. Because of this coverage of climate regimes, the PIRATA buoy data have value for examining the veracity of the WHOI flux product. However, because of the PIRATA wind and air temperature measurements being assimilated in the ECMWF operational forecast model (M. McPhaden

2002, personal communication), the PIRATA data are quasi independent for the validation here.

Clearly, though the measurements were taken at different times of different years and lasted from barely a month to two years, they represent four different meteorological regimes. The diversity in the buoy/ship locations allows the examination of the WHOI fluxes under different climate associations.

4. Evaluation analysis

The following tools are used in the validation analysis: comparison of the time series, comparison between the means averaged over the measurement period, and computation and comparison of the standard deviations (SD) of daily differences, the correlation coefficients (r), and the linear regressions. The time series comparison details the coherence of temporal signals. The mean differences quantify systematic error in the WHOI product. The daily SD quantifies the departure of the WHOI product from the measurements on a daily basis. The correlation coefficient r measures how well the two datasets covary in time. The linear regression line indicates how well the two datasets fit in a linear sense. All the information is presented by using a time series plot, a scatter diagram, and a table.

It should be noted that the paper, like some other flux analysis studies (e.g., Weller and Anderson 1996; Josey 2001; Sun et al. 2003), defines the heat loss from the ocean as negative fluxes and heat gain by the ocean as positive fluxes. Hence, overestimation or underestimation is expressed differently between fluxes (Q_{LH}, Q_{SH}) and basic variables (U, q_a, T_a, and T_s) when discussing the sign of WHOI minus buoy/ship. For fluxes, a negative (positive) sign indicates that the oceanic heat loss is overestimated (underestimated) compared to buoy/ship measurements. For basic variables, a negative (positive) sign indicates that the amplitude of the variable is underestimated (overestimated).

a. The Subduction Experiment array

The comparison of the WHOI latent (Q_{LH}) and sensible (Q_{SH}) fluxes and flux-related surface meteorological variables ($q_s - q_a$, $T_s - T_a$, U, T_s, T_a, q_a) with buoy measurements at the Subduction Experiment site is presented in Figs. 4–5 and Table 2. While the time series plot (Fig. 4) shows the observations obtained at the northeast location (33°N, 22°W), where the record was longest, the scatterplot (Fig. 5) and the statistical information (Table 2) are based on the measurements taken at all five buoys.

Across the Subduction Experiment array, Q_{SH} is significantly smaller than Q_{LH}. The mean of the measured Q_{SH} (-7.56 W m^{-2}) is less than 7% of the mean of the measured Q_{LH} (-103.6 W m^{-2}) over the 2–yr measurement period. The mean differences between the measured and the WHOI-analyzed Q_{LH} and Q_{SH} are 2.94 (3%) and 1.01 W m^{-2} (13%), respectively. These mean errors are within the accuracy of the buoy fluxes estimated by Moyer and Weller (1997). The measured and the analyzed Q_{LH} agree remarkably well. The correlation coefficient (r) is 0.90 and the regression slope is 0.88. By comparison, the Q_{SH} data pair is less close: both r and the slope are lower at 0.77 and 0.74, respectively. This is because the analyzed Q_{SH} often has a phase differing from observation in summertime when the flux values fluctuated near the zero line, though it represents well the timing and amplitude of major synoptic events in fall/winter seasons.

There are two features worth noting when examining the relationship between flux-related variables and fluxes. First, wind speed (U) has a better correlation and higher value of regression slope than air–sea humidity and temperature differences, $q_s - q_a$ and $T_s - T_a$. The better U leads to a better correlation coefficient for both Q_{LH} and Q_{SH}, and the effect is more evident on Q_{LH}. Second, the lower values of the correlation and slope in $q_s - q_a$ and $T_s - T_a$ are not due to the poor estimation of the three basic variables, T_s, T_a, and q_a. In fact, these three variables all have a correlation coefficient higher than 0.90 and a regression slope greater than 0.85. They also have a mean highly consistent with the observed mean: the difference is 0.00°C (0%) for T_s, 0.09°C (0.4%) for T_a, and 0.13 g kg^{-1} (1%) for q_a. It appears that the degraded correlation in $q_s - q_a$ and $T_s - T_a$ is caused primarily by the lack of daily variability in the analyzed T_s. This can be seen in that the analyzed T_a and q_a represent well both the seasonal trend and day-to-day variations, while the analyzed T_s captures only the seasonal trend but not high-frequency signals. As q_s is computed from the saturation mixing ratio for seawater at T_s (Fairall et al. 1996), a smooth T_s leads to a smooth q_s and affects the representation of daily fluctuations in both $q_s - q_a$ and $T_s - T_a$.

The lack of daily variations in the analyzed T_s stems largely from the problem in the T_s from the ECMWF and NCEP2 outputs, as the two model datasets are input data sources, in the WHOI synthesis and their quality has a direct impact on the T_s estimation. The daily T_s used in the ECMWF and NCEP2 assimilation is obtained by interpolating the weekly T_s analysis of Reynolds and Smith (1994), albeit the two models have different interpolation strategies (Sun et al. 2003). Such an approach does not present day-to-day variations in T_s. The AVHRR daily T_s observations, though included in the WHOI synthesis, appear to be insufficient to rectify the problem. The lack of AVHRR observations under cloudy conditions reduces considerably the number of available data points and limits the influence of the AVHRR data on the synthesis. This is further discussed in section 5.

b. The coastal buoys

The comparison at the CMO, SESMOOR, and ASREX buoy sites in the western North Atlantic is sum-

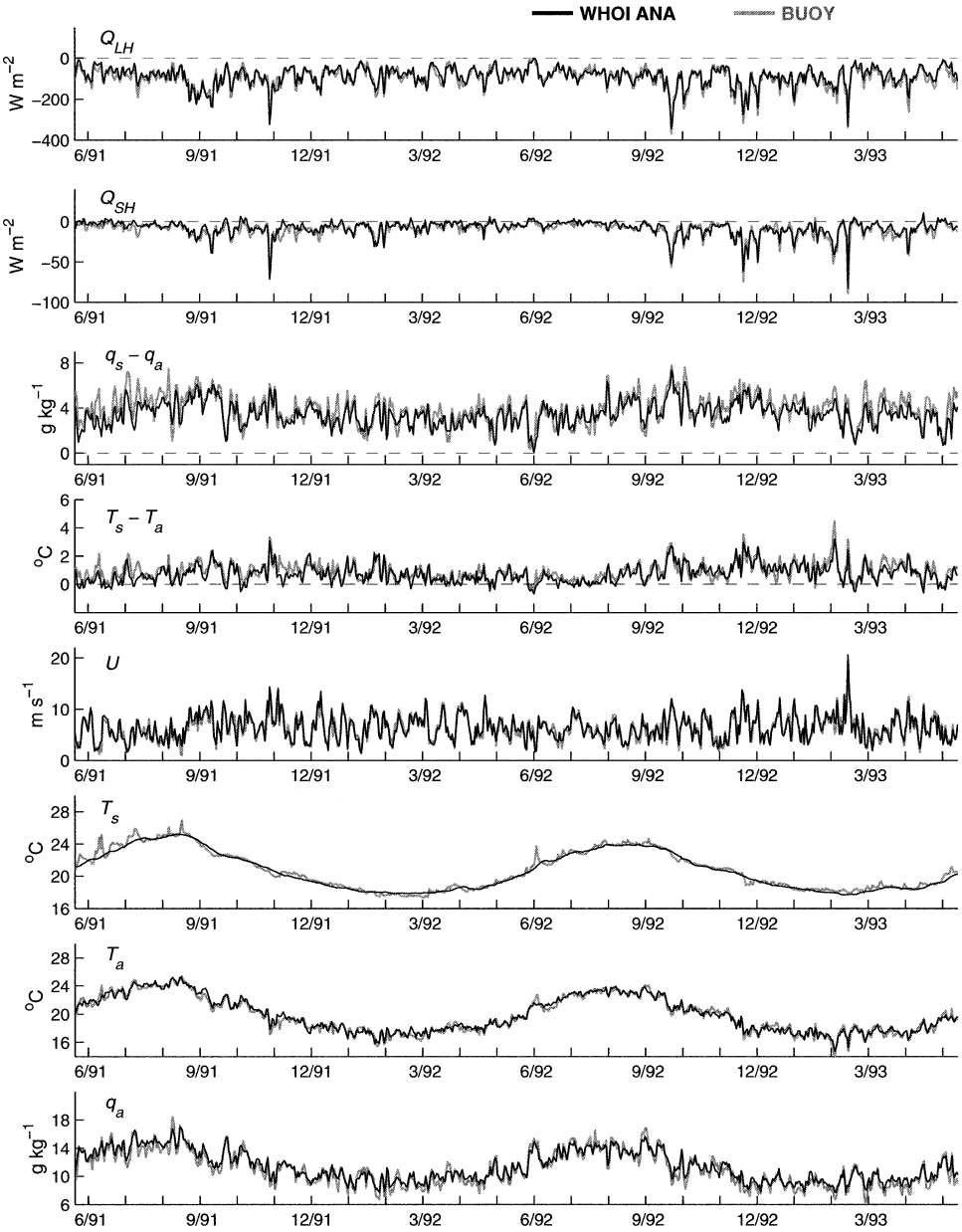

FIG. 4. Time series plots of the measured (gray) and the WHOI-analyzed (dark) latent heat flux (Q_{LH}), sensible heat flux (Q_{SH}), sea–air humidity differences ($q_s - q_a$), sea–air temperature differences ($T_s - T_a$), wind speed at 10 m (U), SST (T_s), air temperature at 2 m (T_a), and air specific humidity at 2 m (q_a) at one Subduction Experiment buoy site (33°N, 22°W).

marized in Figs. 6–7 and Table 3. All three buoys were deployed between the months of October and May, albeit in different years. The timing of the deployment fell within the season that features rapid intensification of cyclones passing through the region. Short duration (2–3 days), strong wind, a large drop in air temperature and humidity, and excessive latent and sensible heat losses from the ocean are the characteristics of the cyclonic storms, which are readily identifiable in the time series plots in Fig. 6.

The timing of synoptic events in Q_{LH} and Q_{SH} is well captured by the WHOI synthesis at the CMO and ASREX sites, but not quite so well at the SESMOOR site. This can also be seen from the values of the correlation coefficient and regression slope, which are very high at CMO and ASREX but low at SESMOOR. At all the three sites, the observed high-frequency variability is well represented by the U, T_a, and q_a estimates but not so well for T_s. The poor T_s estimates appear to be the main reason for the mismatch between analyzed and buoy fluxes. As at the Subduction Experiment site (Fig. 4), the T_s estimate lacks day-to-day variations. But un-

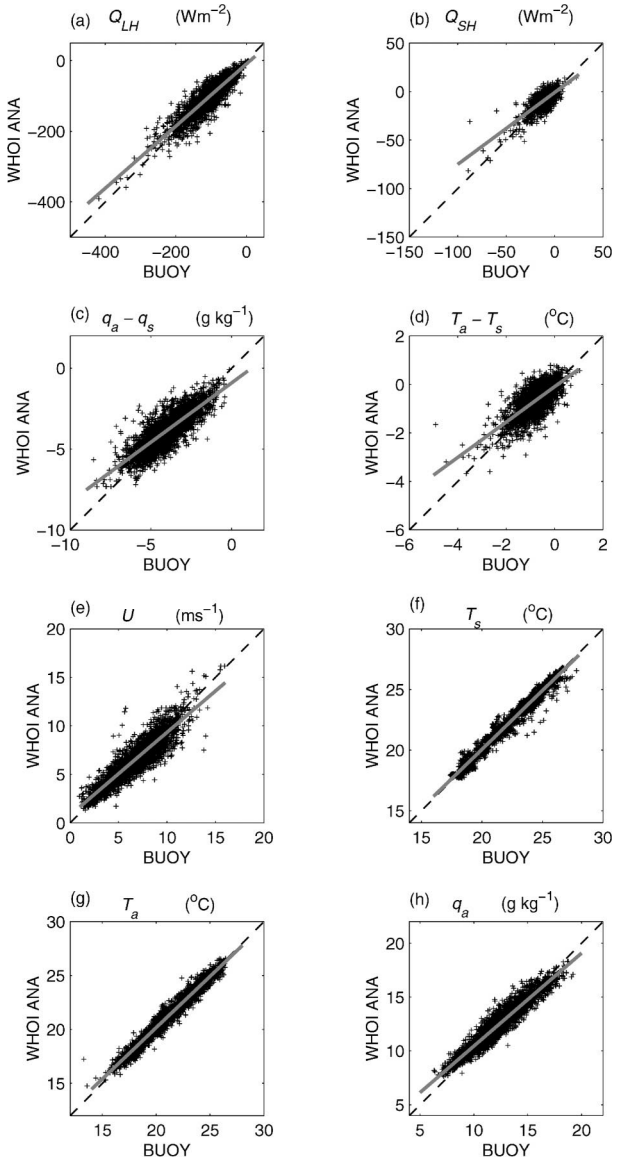

FIG. 5. Scatterplots of buoy observations versus the WHOI-analyzed data constituted at the five buoy sites of the Subduction Experiment. (a) Q_{LH}; (b) Q_{SH}; (c) $q_a - q_s$; (d) $T_a - T_s$; (e) U; (f) T_s; (g) T_a; and (h) q_a. A linear regression line is shown, where the observations are assumed to be independent and the WHOI-analyzed data to be dependent.

like the Subduction Experiment site, the T_s estimate shows also a considerable systematic bias (1.28° at CMO, 2.42° at SESMOOR, and −0.35°C at ASREX). The difference is particularly pronounced at SESMOOR where the estimated T_s is smooth but the buoy T_s showed considerable variability. Major drops in buoy T_s were evident around 26 November, 17 December, and 5 January, each associated with large Q_{LH} and Q_{SH} loss from the ocean. The event around 5 January registered the largest sensible heat loss (~ -380 W m^{-2}) during the entire SESMOOR record with $T_s - T_a$ of up to 12°C. This large anomaly was attributable to a concurrent warm-core ocean eddy passing through the buoy location (Crescenti and Weller 1992) that caused an abrupt jump in T_s preceding the passing of a storm. However, none of these steplike changes were present in the analyzed T_s.

The analyzed T_s is biased warm at the CMO and SESMOOR sites by 1.28° and 2.42°C, respectively. This bias dominates the warm bias in the analyzed T_a, resulting in larger ($T_s - T_a$) and stronger Q_{SH}. It also causes a large wet bias in q_s that increases ($q_s - q_a$) and boosts Q_{LH}. The overestimation biases in Q_{LH} and Q_{SH}, respectively, are 20.42 and 7.32 W m^{-2} at CMO and 16.34 and 18.57 W m^{-2} at SESMOOR. The large warm T_s biases are attributable to the coarse resolution in the NCEP2 (1.875° by 1.875° grid) and ECMWF (1.125° by 1.125° grid) models, which is insufficient to resolve the sharp thermal gradient surrounding the two buoy sites (Sun et al. 2003). The CMO buoy was located on the continental shelf and was about 100 km away from the northern boundary of the Gulf Stream. The SESMOOR buoy was about 300 km southeast of Halifax, Nova Scotia, in 2984 m of water and was bounded to the south by the Gulf Stream. We notice that the T_s bias also influences the estimation of the 2-m T_a in the NWP models. The 2-m T_a is obtained by interpolating between the lowest model level (about 30 m for the ECMWF model and 50 m for the NCEP2 model) and the surface using a stability-dependent surface layer scheme (Kanamitsu 1989; Kalnay et al. 1996). It is not surprising to see that the biases in T_a and T_s estimates have the same sign at all measurement locations.

c. *The* Knorr *cruises*

The evaluation of the WHOI analysis product along the two cruise tracks of the R/V *Knorr* is presented in Figs. 8–9 and Table 4. Weather conditions during the two cruises were quite different. The cruise in February–March 1997 experienced continual cold air outbreaks that brought cold, dry air masses over the Labrador Sea, but the cruise in January–February 1998 had relatively calm weather most of the time, with only a few brief (1–2-day duration) cold air outbreaks recorded. Extremely large sensible (greater than 400 W m^{-2}) and latent (greater than 200 W m^{-2}) heat losses were observed during the first cruise, while moderate sensible (less than 200 W m^{-2}) and latent (less than 150 W m^{-2}) heat exchanges prevailed during the second cruise.

The cold air outbreak situation is typified by high wind speed, low air temperature, and low air humidity. These events can be readily identified from the time series plots in Fig. 8. Compared to ship measurements acquired from the two cruises, the analyzed q_a replicates the timing and magnitude of synoptic variations. The analyzed T_a is reasonably good; the only problem is that the timing of peaks occasionally lags behind that of the observations. The analyzed T_s and U are less good; T_s

TABLE 2. Statistics and regression based on comparisons between daily buoy measurements and daily WHOI flux product at the Subduction Experiment site (5-buoy array, total sample size = 2640 days).

Variable	WHOI mean	OBS mean	Difference		Correlation coefficient	Regression*	
			Mean	Std dev		c_1	c_0
Q_{LH} (W m^{-2})	−100.67	−103.61	2.94	21.52	0.90	0.88	−9.55
Q_{SH} (W m^{-2})	−6.54	−7.56	1.01	5.20	0.77	0.74	−0.95
$q_s - q_a$ (g kg^{-1})	3.81	3.94	−0.13	0.73	0.83	0.73	0.91
$T_s - T_a$ (°C)	0.62	0.72	−0.10	0.43	0.72	0.73	0.10
U (m s^{-1})	6.62	6.84	−0.22	1.03	0.90	0.85	0.78
T_s (°C)	22.12	22.12	0.00	0.41	0.98	0.97	0.64
T_a (°C)	21.49	21.40	0.09	0.48	0.98	0.95	1.12
q_a (g kg^{-1})	12.47	12.34	0.13	0.71	0.95	0.86	1.83

* WHOI flux = $c_1 \times$ OBS + c_0 (linear regression).

is persistently colder and U is mostly stronger than their measurement counterparts. The degree of replication can be seen from the value of the correlation coefficient, which is high for q_a (0.96) and T_a (0.94) but rather low for T_s (0.39) and U (0.53). The estimates for the latter two variables also have a relatively large scatter with respect to the observations (Fig. 9).

The cause of the cold bias in the analyzed T_s is largely attributable to the cold biased T_s from the ECMWF and NCEP2 outputs. Renfrew et al. (2002) showed that two factors, namely, insufficient T_s observations and the crude representation of the model's sea ice edge, affect the NWP model T_s in the Labrador Sea. SST observations are needed in the assimilation to provide model constraints, but both ship data and satellite retrievals are limited in wintertime. At data-void points, T_s is determined by an interpolation from the model's sea ice edge to the nearest available data point (ECMWF 1994; Kalnay et al. 1996). The model's sea ice mask is determined from the sea ice concentration remotely sensed by SSM/I, but the implementation is rather crude. It maps the SSM/I data with a resolution of 25 km to the coarse model resolution (~1.125° for ECMWF and ~1.875° for NCEP2) and then only uses a 0% or 100% flag for the ice cover (ECMWF 1994; Kalnay et al. 1996). Renfrew et al. (2002) showed that the track of the R/V *Knorr* cruise in 1997 was sometimes in the marginal ice zone, the region that is defined as the ice edge by NWP models. The mismatch in the observed and modeled sea ice cover leads to cold biased T_s at these locations. This inevitably affects the T_s estimation in the synthesis.

Interestingly, errors in different variables can compensate each other and make the variable combination agree better with the observation counterpart. This is most noticeable in $T_s - T_a$, which is less biased and better correlated than either individual component.The effect is also seen in the Q_{LH} calculation, particularly for 1997. The multiplication between persistently dry biased $q_s - q_a$, which results from the cold biased T_s, and persistently strong biased U produces a Q_{LH} that matches quite well with the Q_{LH} estimated from the ship measurements.

d. The PIRATA array

The measurement time series for basic variables and latent and sensible heat fluxes at two PIRATA buoy locations, (15°N, 38°W) and (10°S, 10°W), are shown in Figs. 10a,b along with the time series from the WHOI synthesis. The scatterplot in Fig. 11 and the statistical and regression analysis in Table 5 are based on the measurements from all 11 buoys.

The time series comparisons reveal three outstanding features. First, the bias in the $q_s - q_a$ estimate has more to do with q_a than with T_s. This is quite different from the findings at the coastal buoys (CMO, SESMOOR, ASREX) and along the *Knorr* ship tracks, where the bias in T_s is the main cause for the bias in $q_s - q_a$. It appears that the analyzed q_a is biased dry across the PIRATA array. The comparison study of Sun et al. (2003) found that the mean q_a that was averaged over the same 11 PIRATA buoys and over the same period is underestimated by 1.0 g kg^{-1} by ECMWF and by 0.3 g kg^{-1} by NCEP2. The analyzed q_a has an underestimated bias of 0.55 g kg^{-1}. It appears that the analyzed q_a is affected by the systematic biases in q_a from the two NWP models. Second, the analyzed $T_s - T_a$, though having a very small bias (0.01°C), is poorly correlated with the observational counterpart ($r = 0.49$). This can be seen from Figs. 10a,b that the estimated T_s and T_a are both good in representing the low-frequency seasonal trend but poor in representing day-to-day variations. Last, the heat loss by Q_{LH} and Q_{SH} are overestimated by 11.94 and 0.71 W m^{-2}, respectively. The error structures in Q_{LH} and Q_{SH} reflect largely those in $q_s - q_a$ and $T_s - T_a$. The scatterplot in Fig. 11, which is based on all measurements, shows that Q_{LH} and $q_s - q_a$ have a similar scatter structure. The same is also true for the Q_{SH} and $T_s - T_a$ pair.

5. Discussion

The analysis indicates that T_s is the least well represented variable in the WHOI analysis and that the errors in T_s affect the synthesized Q_{LH} and Q_{SH} estimates. The effect is particularly pronounced at the western

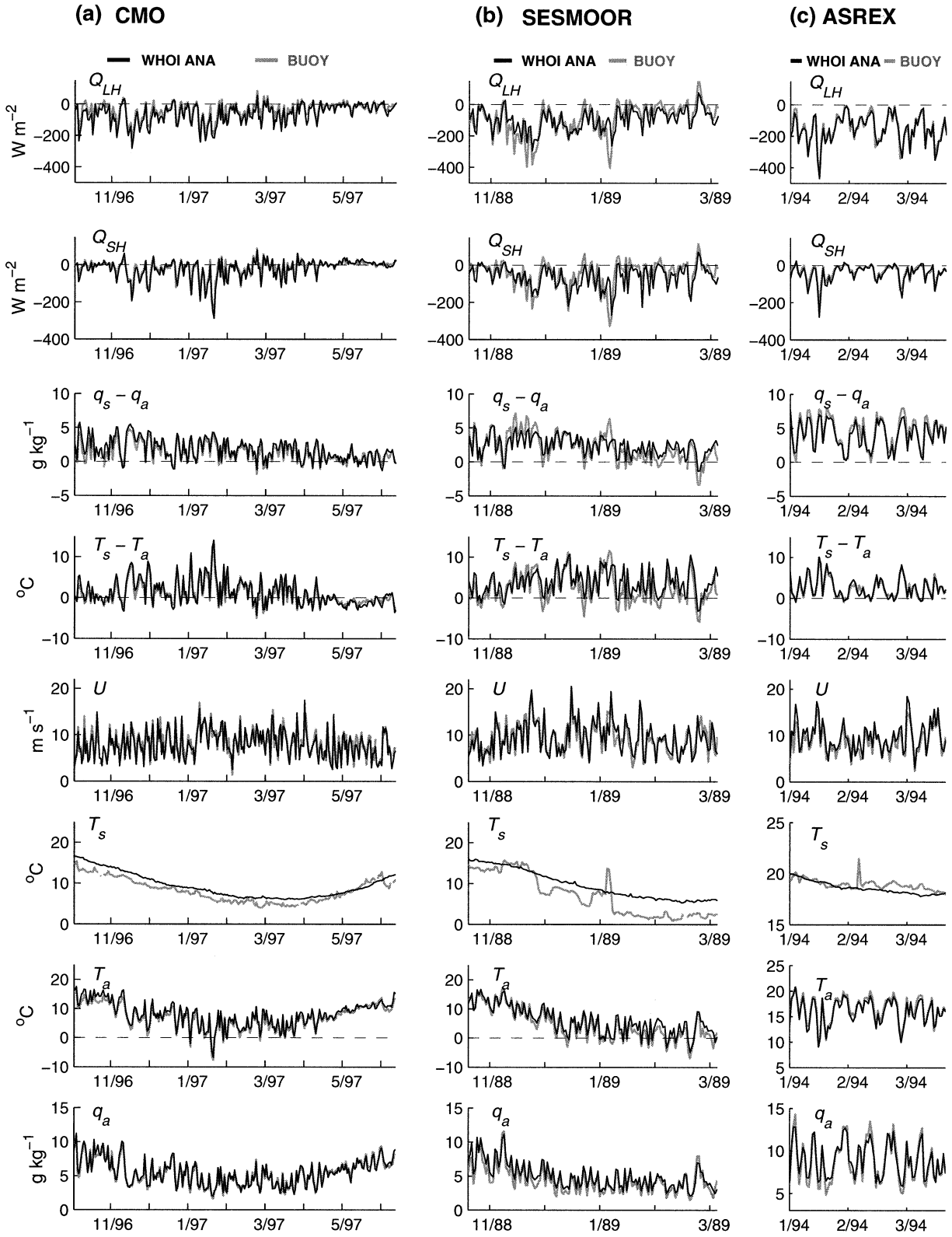

FIG. 6. As in Fig. 4 but for (a) the CMO site, (b) the SESMOOR site, and (c) the ASREX site.

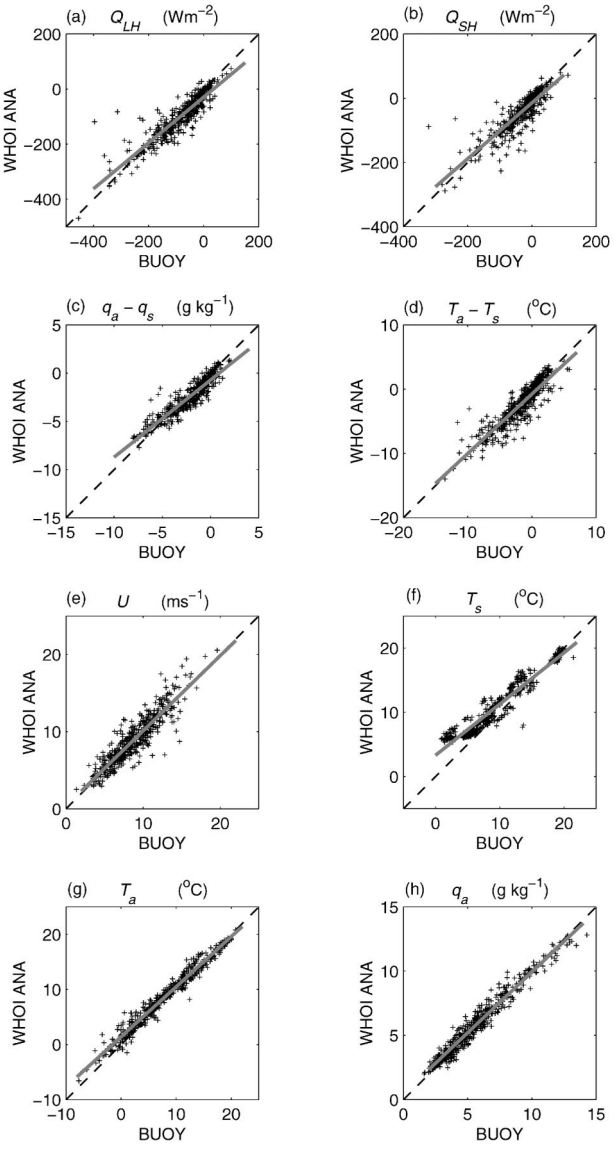

FIG. 7. As in Fig. 5 but constituted at the sites of the three coastal buoys (CMO, SESMOOR, ASREX).

North Atlantic coastal buoy sites and along the ship tracks in the Labrador Sea. The q_a estimate is generally realistic outside of the Tropics but appears to be biased dry across the PIRATA array in the tropical Atlantic. The analysis also indicates that the poor T_s and q_a estimation is primarily attributable to the problems in the NWP models. Since the variables estimated from the WHOI analysis result from the synthesis process that includes not only the NWP outputs but also satellite observations, one natural question is how much do satellite data influence the synthesis process. Furthermore, since the synthesized variables represent the best estimate with least error variance among all the input data, the other question is how much is the WHOI synthesis improved over the NWP model variables. The two questions are addressed in this section. In the following, plots are made at the four major experiment sites: the Subduction Experiment array (SUBDUC: five buoys), the western North Atlantic coastal region (COAST: three buoys), the *Knorr* ship tracks (KNORR: two cruises), and the PIRATA array (PIRATA: 11 buoys).

a. The influence of satellite data on the synthesis

The satellite observations included in the WHOI synthesis (Yu et al. 2004) are daily 10-m U and q_a derived from SSMI (Wentz 1997; Chou et al. 2003) and daily T_s derived from AVHRR (Brown et al. 1993). The 10-m q_a is height adjusted to the 2-m q_a using the COARE2.6a algorithm before being synthesized. The percentage of the length of available satellite data relative to in situ measurement periods is plotted in Fig. 12.

Although the satellite that carries the AVHRR scanner orbits the earth 14 times each day from 833 km above the surface and each pass of the satellite provides a 2399-km-wide swath (Brown et al. 1993), the availability of the AVHRR T_s at all four experiment sites is generally low. It covers 55% of the total 2640 sampling days over the five-buoy Subduction Experiment array, 50% of the total 437 sampling days at the three coastal buoy sites, 12% of the total 61 sampling days during the two R/V *Knorr* cruises, and 30% of the total 2527

TABLE 3a. Statistics and regression based on comparisons between daily buoy measurements and daily WHOI flux product at CMO (sample size = 226 days).

Variable	WHOI mean	OBS mean	Difference		Correlation coefficient	Regression*	
			Mean	Std dev		c_1	c_0
Q_{LH} (W m^{-2})	−69.64	−49.21	−20.42	18.66	0.96	1.07	−17.18
Q_{SH} (W m^{-2})	−26.93	−19.61	−7.32	14.91	0.96	1.04	−6.46
$q_s - q_a$ (g kg^{-1})	1.92	1.45	0.46	0.50	0.94	1.08	0.35
$T_s - T_a$ (°C)	1.58	1.12	0.45	0.84	0.95	1.10	0.34
U (m s^{-1})	8.31	8.51	−0.20	1.10	0.92	0.97	0.08
T_s (°C)	9.35	8.06	1.28	0.85	0.96	1.02	1.11
T_a (°C)	7.77	6.94	0.83	0.69	0.99	1.03	0.63
q_a (g kg^{-1})	5.32	5.29	0.03	0.37	0.98	1.00	0.03

* WHOI flux = $c_1 \times$ OBS + c_0 (linear regression).

TABLE 3b. Statistics and regression based on comparisons between daily buoy measurements and daily WHOI flux product at SESMOOR (sample size = 129 days).

Variable	WHOI mean	OBS mean	Difference		Correlation coefficient	Regression	
			Mean	Std dev		c_1	c_0
Q_{LH} (W m^{-2})	−104.06	−87.72	−16.34	57.66	0.77	0.57	−53.70
Q_{SH} (W m^{-2})	−67.02	−48.45	−18.57	49.58	0.73	0.61	−37.41
$q_s - q_a$ (g kg^{-1})	2.54	2.13	0.41	1.04	0.84	0.63	1.21
$T_s - T_a$ (°C)	3.97	2.68	1.29	2.18	0.81	0.67	2.17
U (m s^{-1})	9.58	9.40	0.18	1.70	0.88	0.93	0.88
T_s (°C)	9.72	7.30	2.42	2.15	0.93	0.65	4.99
T_a (°C)	5.75	4.62	1.13	1.58	0.96	0.87	1.76
q_a (g kg^{-1})	4.93	4.53	0.40	0.58	0.95	0.94	0.68

sampling days over the 11-buoy PIRATA array. The major factor affecting the T_s retrieval from AVHRR measurements is the presence of clouds. Hence, the amount of available AVHRR T_s was dramatically reduced at locations frequented by cyclones. This is obvious at the SESMOOR site where the AVHRR T_s were available for only 35 days during the 129-day buoy deployment. This is also seen along the R/V *Knorr* cruise tracks where only two data values exist during the 36-day cruise in 1997 and six values during the 29-day cruise in 1998. For those grid points without AVHRR data, the WHOI synthesis depends on the T_s values from the NCEP2 and ECMWF outputs to obtain an estimate for T_s. As discussed in the previous section, the estimated T_s is biased warm at SESMOOR (Fig. 6) because the resolution used in the NWP models is too coarse to resolve the Gulf Stream front. The estimated T_s is biased cold along the *Knorr* cruise tracks (Fig. 8) because the sea ice mask used in the NWP models is too crude to resolve the marginal ice zone.

The spacecraft carrying SSM/I is in a circular sun-synchronous near-polar orbit at an altitude of approximately 860 km and an orbit period of 102 min similar to AVHRR. The 1394-km swath of the SSM/I, only half of that of AVHRR, can cover 82% of the earth's surface between 87°36′S and 87°36′N in 24 h. Known factors that affect the SSM/I retrievals include rain, because the Wentz algorithm (1997) degrades when cloud/rain liquid water values exceed 18 mg cm^{-3}, and sea ice, because the retrieval algorithm has not been fully validated over these areas. The SSM/I q_a was estimated by Chou et al. (2003) from the total precipitable water over the open ocean (Wentz 1997) and the precipitable water in the lower 500 m of the atmospheric boundary layer (Schulz et al. 1993) using an empirical orthogonal function (EOF) method (Chou et al. 1997). Except along the *Knorr* cruises, the percentage of available SSM/I q_a is very similar to that of SSM/I U, both at more than an 80% level. The SSM/I q_a is extremely limited along the two *Knorr* cruises, only 2 days in the 1997 cruise and 4 days in the 1998 cruise. The low q_a availability in the Labrador Sea was believed due to the coarser sea ice mask used by Chou et al. in producing their 1° gridded fields.

It is worth noting that, unlike the AVHRR T_s that goes directly to the NWP data assimilation systems, the SSM/I q_a from the Chou et al. analysis is not assimilated by the NWP models. Along the *Knorr* ship tracks where both q_a and T_s observations are limited, the WHOI analysis depends largely on the performance of the NWP models. The analyzed q_a agrees well with the ship-observed q_a (Fig. 8 and Table 4) because the NWP models have good q_a estimates, whereas the analyzed T_s has a large cold bias because the NWP models have poor T_s estimates. Yet, high availability of SSM/I q_a does not always mean that it can improve the synthesis. We have shown that the WHOI estimated q_a has an overall underestimation (dry) bias (by 0.55 g kg^{-1}) in the tropical Atlantic (Figs. 10a,b and Table 5). We have found that both ECMWF and NCEP2 models produce an underestimated q_a with a respective value of 1.0 and 0.3 g kg^{-1} (Sun et al. 2003). We note that the SSM/I q_a, with

TABLE 3c. Statistics and regression based on comparisons between daily buoy measurements and daily WHOI flux product at ASREX (sample size = 82 days).

Variable	WHOI mean	OBS mean	Difference		Correlation coefficient	Regression	
			Mean	Std dev		c_1	c_0
Q_{LH} (W m^{-2})	−155.89	−152.61	−3.28	23.72	0.97	0.96	−9.29
Q_{SH} (W m^{-2})	−41.94	−34.99	−6.96	13.57	0.97	1.14	−2.08
$q_s - q_a$ (g kg^{-1})	4.02	4.47	−0.45	0.61	0.97	0.85	0.20
$T_s - T_a$ (°C)	2.63	2.50	0.13	0.65	0.97	1.05	0.00
U (m s^{-1})	9.70	8.78	0.92	1.09	0.94	1.06	0.35
T_s (°C)	18.61	18.95	−0.35	0.49	0.61	0.70	5.34
T_a (°C)	15.98	16.45	−0.47	0.47	0.98	0.98	−0.16
q_a (g kg^{-1})	8.95	8.79	0.16	0.63	0.98	0.81	1.83

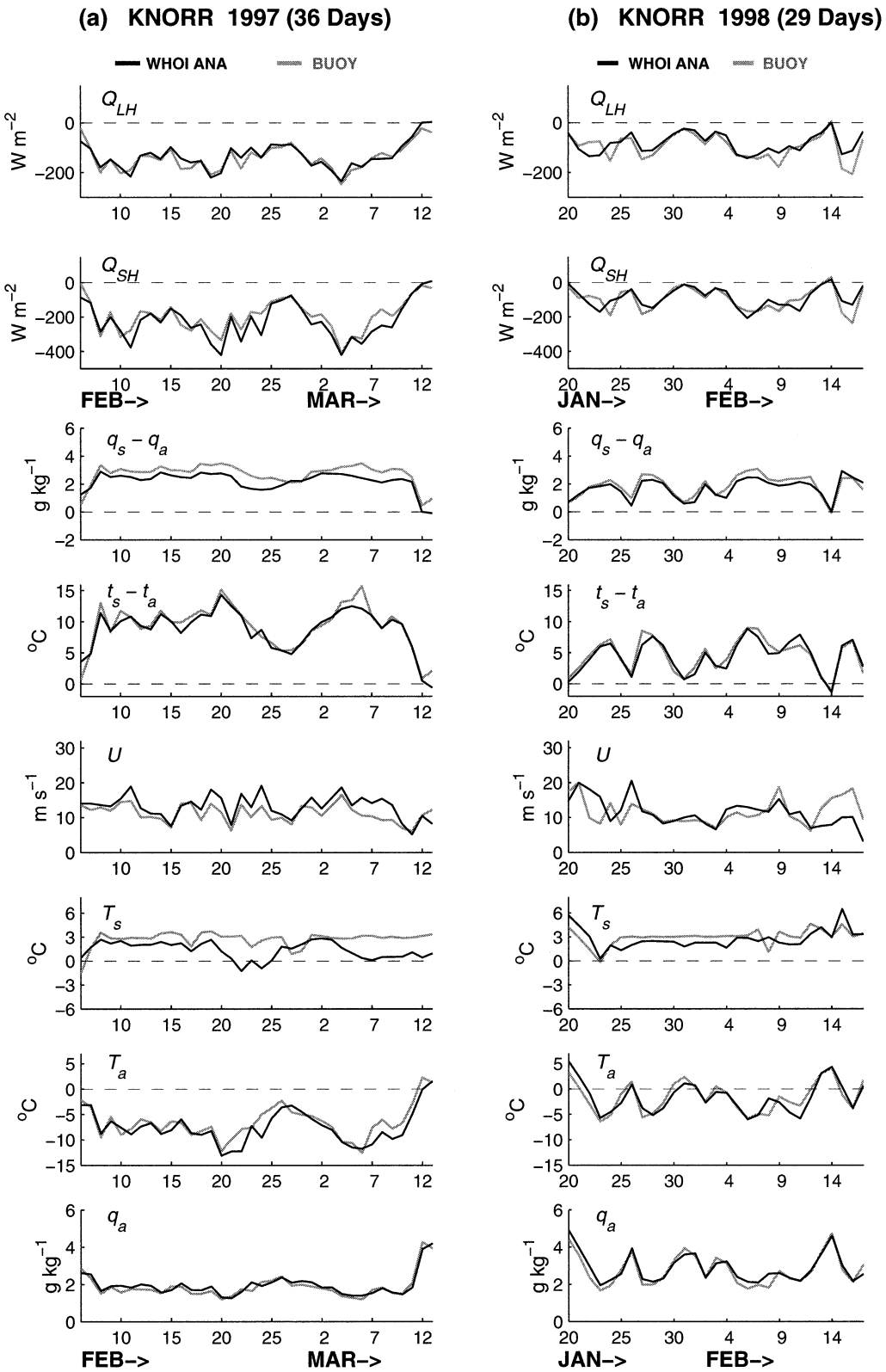

FIG. 8. As in Fig. 4 but along the *Knorr* cruise tracks during (a) 8 Feb–13 Mar 1997, and (b) 24 Jan–13 Feb 1998.

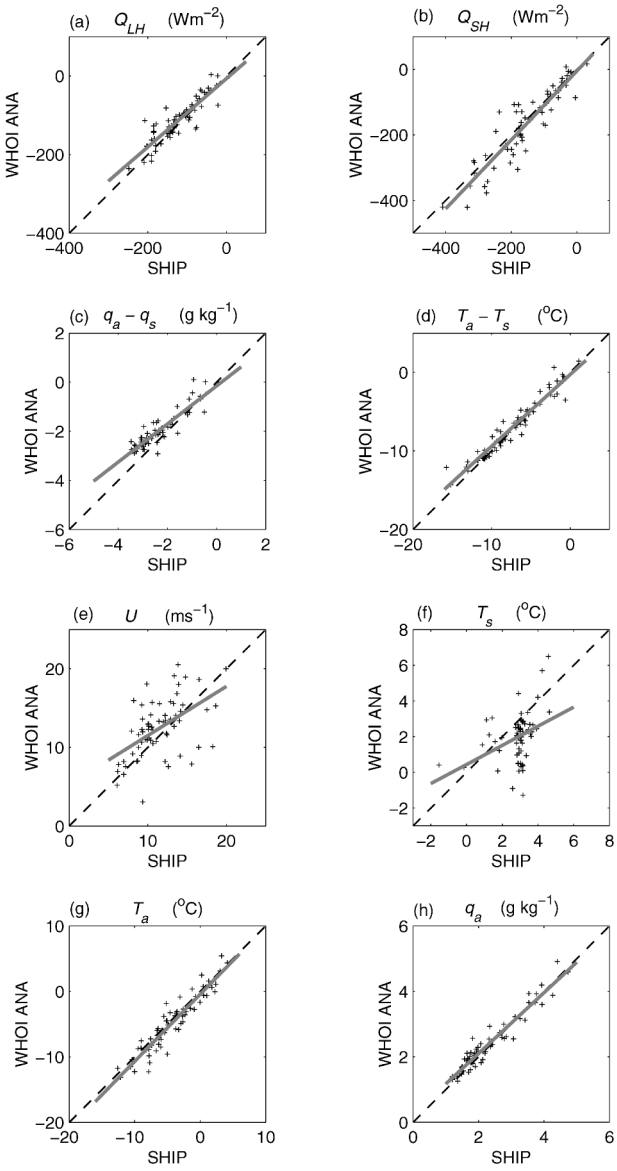

FIG. 9. As in Fig. 5 but constituted along the two *Knorr* cruise tracks.

a mean of 16.15 g kg^{-1} averaged over the 11 PIRATA buoys, is also biased dry by 0.86 g kg^{-1} for unknown reasons.

b. The improvement over the NWP outputs

The ECMWF and NCEP2 basic variables are part of input data for the WHOI synthesis and so they cannot be used as validation datasets. They are useful, however, in assessing the degree of improvement made by the WHOI synthesis and in diagnosing whether and how further improvements can be implemented. The WHOI fluxes are calculated based on the COARE flux algorithm 2.6a, different from those used in the ECMWF and NCEP2 models. The study of Sun et al. (2003) indicated that the deficiencies in the flux parameterization schemes have a contribution to the errors in the NWP latent and sensible heat fluxes equal to that of the errors in the surface meteorological variables. The problems in the NWP flux algorithms are beyond the scope of this study; the reader is referred to Brunke et al. (2003) for general discussions and Sun et al. (2003) for quantification analysis. The present study focuses on assessing the improvement of the WHOI basic variables over the NWP basic variables. To do so, two bar plots are made over in situ measurement periods summed over the total number of buoys/ship tracks included in each experiment. The mean differences between the measured daily latent and sensible heat fluxes and basic variables and those from the WHOI analysis, and the ECMWF and NCEP2 outputs are shown in Fig. 13, while the standard deviations of the daily differences are shown in Fig. 14. The evaluation is summarized as follows.

1) LATENT AND SENSIBLE HEAT FLUXES

Q_{LH}: Compared to the measurement values, the WHOI analyzed mean Q_{LH} is underestimated by 2.9 W m^{-2} (2% of the measurement mean value) at SUBDUC and 8.7 W m^{-2} (7%) at KNORR, while it is overestimated by 11.9 W m^{-2} (11%) at PIRATA and 15.9 W m^{-2} (20%) at COAST. ECMWF and NCEP2 overesti-

TABLE 4. Statistics and regression based on comparisons between daily ship measurements and daily WHOI flux product along the *Knorr* ship tracks (two ship tracks, total sample size = 65 days).

Variable	WHOI mean	OBS mean	Difference		Correlation coefficient	Regression*	
			Mean	Std dev		c_1	c_0
Q_{LH} (W m^{-2})	−111.00	−119.79	8.79	25.90	0.89	0.87	−6.97
Q_{SH} (W m^{-2})	−159.45	−149.71	−9.74	44.81	0.92	1.05	−5.11
$q_s - q_a$ (g kg^{-1})	1.96	2.33	−0.37	0.36	0.91	1.02	0.44
$T_s - T_a$ (°C)	6.83	7.17	−0.34	1.01	0.97	0.93	−0.24
U (m s^{-1})	11.89	11.43	0.46	3.25	0.53	0.63	5.25
T_s (°C)	1.97	2.86	−0.88	1.31	0.39	0.54	0.44
T_a (°C)	−4.85	−4.31	−0.55	1.30	0.94	1.02	−0.44
q_a (g kg^{-1})	2.36	2.28	0.05	0.24	0.96	0.93	0.24

* WHOI flux = $c_1 \times$ OBS + c_0 (linear regression).

TABLE 5. Statistics and regression based on comparisons between daily ship measurements and daily WHOI flux product at the PIRATA array (11 buoys; total sample size = 2527 days).

Variable	WHOI mean	OBS mean	Difference		Correlation coefficient	Regression*	
			Mean	Std dev		c_1	c_0
Q_{LH} (W m^{-2})	−119.11	−107.17	−11.94	25.44	0.77	0.70	−50.23
Q_{SH} (W m^{-2})	−6.21	−5.50	−0.71	4.97	0.49	0.49	−3.52
$q_s - q_a$ (g kg^{-1})	4.40	4.18	0.32	0.82	0.70	0.52	2.51
$T_s - T_a$ (°C)	0.58	0.57	0.01	0.45	0.49	0.42	0.34
U (m s^{-1})	6.94	6.92	0.03	0.85	0.88	0.82	1.26
T_s (°C)	26.42	26.44	−0.02	0.37	0.97	0.96	1.09
T_a (°C)	25.84	25.87	−0.03	0.46	0.96	0.98	0.42
q_a (g kg^{-1})	16.46	17.01	−0.55	0.66	0.95	0.82	2.58

* WHOI flux = $c_1 \times$ OBS + c_0 (linear regression).

mate the latent heat losses from the ocean at all measurement sites. The overestimation by ECMWF/NCEP2 is 16.5/11.5 W m^{-2} (16%/11%) at SUBDUC, 43.9/40.7 W m^{-2} (55%/51%) at COAST, 6.6/27.5 W m^{-2} (5%/23%) at KNORR, and 36.2/34.7 W m^{-2} (34%/32%) at PIRATA. For the two NWP products, the largest bias is in the western coastal area, and the second largest is in the tropical region. The bias in the WHOI Q_{LH} for these two regions is significantly smaller. The bar plot of the SD of daily differences shows that the WHOI Q_{LH} has a daily variability most consistent with that of the measurements at all measurement sites.

Q_{SH}: The mean Q_{SH} from the WHOI analysis differs from the measurement value by less than 1 W m^{-2} (13%) at SUBDUC and PIRATA, while it is overestimated by 10.5 W m^{-2} (34%) at COAST and by 9.7 W m^{-2} (6%) at KNORR. The NCEP2 Q_{SH} has a mean value similar to the WHOI analysis at SUBDUC and PIRATA, but it considerably overestimates at COAST by 18.0 W m^{-2} (58%) and at KNORR by 58.0 W m^{-2} (39%). By comparison, the ECMWF mean Q_{SH} is only close at KNORR and is the most biased product at the other three regions. Similar to Q_{LH}, the WHOI Q_{SH} has also the smallest SD value at all measurement sites.

2) BASIC VARIABLES

U: The mean difference between the WHOI analysis and the measurements is less than 0.5 m s^{-1} (4%) at all locations. The WHOI analysis gives the best estimation of both mean and daily variability at all buoy sites, but not along the *Knorr* cruise tracks where the ECMWF estimates are slightly better. Of all three products, the NCEP2 estimates appear to be the least representative. The mean difference at KNORR is as high as 1.9 m s^{-1}, accounting for more than 16% of the measurement mean value.

q_a: The WHOI estimates have a slight wet bias (less than 0.16 g kg^{-1}) in the extratropical region, while a slight dry bias (0.55 g kg^{-1}) across the tropical PIRATA array. Compared to the measurement mean values, the biases are small: 1% at SUBDUC, 2.8% at COAST, 3.6% at KNORR, and 3.3% at PIRATA. All three products are biased dry at PIRATA, where the WHOI analysis has improved the representativeness of daily fluctuations but not the mean.

T_a and T_s: The mean T_a and T_s estimates from the three products all agree well with the measurements at SUBDUC and PIRATA, but all are biased warm at COAST and biased cold at KNORR with the NCEP2 T_a at KNORR the only exception. The model deficiencies (i.e., model resolution, sea ice mask) that caused the biases at the latter two locations have been discussed in sections 4b–c, and the discussion has included also the connection between T_a and T_s in the NWP model computations. It appears that the improvement of the T_s and 2-m T_a estimates by the WHOI analysis is small, as there is a lack of sufficient satellite observations for these two variables. The bias in the WHOI T_a is 0.68°C (8%) at COAST and −0.55°C at KNORR (12%), while the bias in the WHOI T_s is 1.3°C (13%) at COAST and −0.88°C (31%) at KNORR. The biases at SUBDUC and PIRATA are all less than 1% of the measurement mean values.

3) VARIABLE COMBINATION

$q_s - q_a$: The mean bias from the WHOI analysis is within ±0.35 g kg^{-1} (15%) at all measurement sites, smaller than both the ECMWF (ranging from −0.2 to 1.2 g kg^{-1}) and NCEP2 (ranging from −0.55 to 0.24 g kg^{-1}) outputs. The smallest SD values also suggest that daily variations are best represented by the WHOI analysis. The bias in T_s has a clear effect on the estimates of $q_s - q_a$. This is most evident at COAST, where the warmer T_s produced a wetter q_s and a wet bias in $q_s - q_a$.

$T_s - T_a$: The mean bias in this quantity reflects largely the mean bias in T_s, particularly at COAST and KNORR. The compensation effect in errors is clearly shown. For instance, $T_s - T_a$ is biased in a lesser degree than T_s for both WHOI and ECMWF at KNORR because the biases in T_s and T_a have the same sign, while it is opposite for NCEP2 because the biases in T_s and T_a have the opposite sign.

$U(q_s - q_a)$: This quantity computed from the WHOI

analysis has the smallest SD values at all the measurement locations. Its mean bias accounts for 4% of the mean measurement value at SUBDUCT, 12% at COAST, 6% at KNORR, and 2% at PIRATA. The ECMWF is most biased (34%) at COAST, and the NCEP2 is most biased (11%) at SUBDUC. Although the NCEP2 is less biased than the ECMWF, daily variations are least well represented by NCEP2. It is worth noting that the bias in this quantity has the same sign as the bias in Q_{LH} for the WHOI estimates, but it is not necessarily so for the ECMWF and NCEP2 outputs (Figs. 13a,i). The latter is apparently caused by the deficiencies in the two NWP bulk flux algorithms.

$U(T_s - T_a)$: The mean bias produced by the WHOI analysis accounts for about 15% of the mean measurement value at SUBDUC, 29% at COAST, 3% at KNORR, and 8% at PIRATA. Overall, ECMWF is most biased and NCEP2 is slightly less biased. Again, the bulk algorithms in ECMWF and NCEP2 distort the relationship between this quantity and Q_{SH}, as the two have the same sign from the WHOI analysis but not so from the ECMWF and NCEP2 models (Figs. 13b,j).

6. Summary and conclusions

Daily latent and sensible heat fluxes for the Atlantic Ocean from 1988 to 1999 with $1^\circ \times 1^\circ$ resolution have been recently developed at WHOI (Yu et al. 2004). The fluxes were constructed by using the surface metrological variables determined from an objective analysis and the state-of-the art TOGA COARE flux algorithm 2.6a. The present study evaluated the degree of improvement made by the WHOI analysis with in situ buoy/ship measurements as verification data. The differences of the WHOI analyzed fluxes and surface meteorological variables from the measurement values were quantified. The comparisons with the ECMWF and NCEP outputs were also included.

The field experiments used in the study included: the five-buoy Subduction Experiment in the eastern subtropical North Atlantic, three coastal region field programs (CMO, SESMOOR, and ASREX) in the western North Atlantic, two winter cruises by R/V *Knorr* from the Labrador Sea Deep Convection Experiment, and 11 PIRATA buoys. The comparisons of the WHOI analysis with the measurements at the four regions are summarized as follows.

a. *The five buoys of the Subduction Experiment in the eastern subtropical North Atlantic*

The mean values of the WHOI basic variables averaged over the measurement periods agree well with those of the measurements. Except that the T_s estimates captured only seasonal variations, the estimates for U, T_a, and q_a represent well both the observed seasonal trend and day-to-day fluctuations. The lack of daily variations in the T_s estimates is largely due to the lack of such variability in the ECMWF and NCEP2 T_s outputs. The AVHRR T_s observations, though used in the synthesis, were available for only 55% of the measurement time and were not sufficient to rectify the problem. However, the smooth T_s estimates did not pose a major problem for the flux estimation at this site, largely because the winds are mild and the magnitude of the daily $T_s - T_a$ fluctuations is small, so the sensible heat flux is small. For instance, the measured mean Q_{SH} (-7.56 W m^{-2}) is less than 7% of the measured mean Q_{LH} (-103.6 W m^{-2}). The mean error for Q_{LH} is 2.94

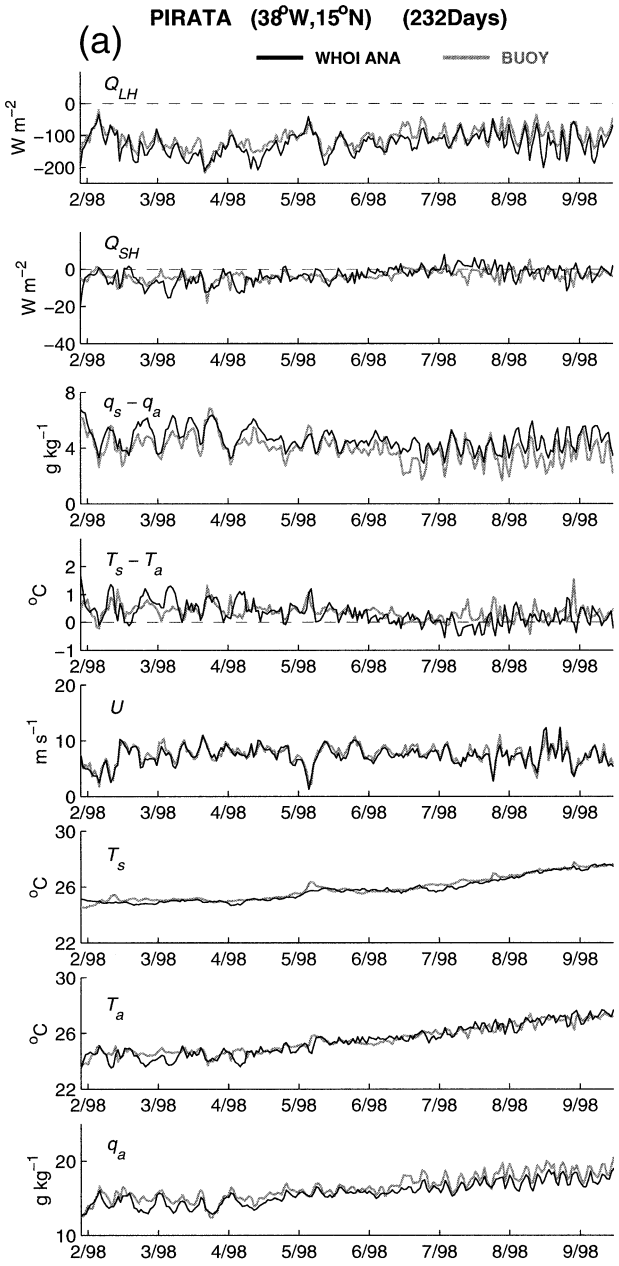

FIG. 10. As in Fig. 4 but for the PIRATA buoy at the location (a) 15°N, 38°W, and (b) 10°S, 10°W.

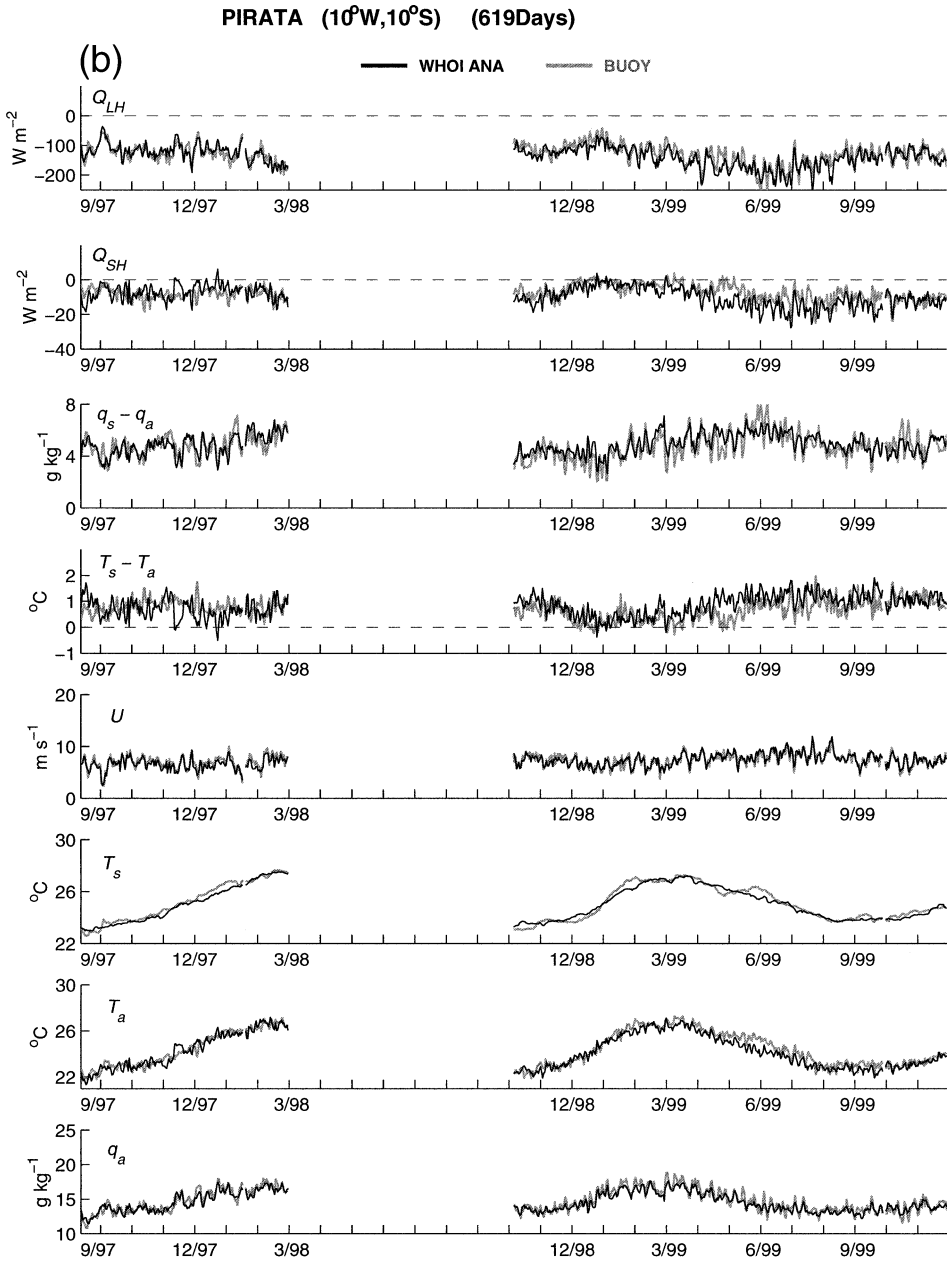

FIG. 10. (*Continued*)

W m^{-2} (3%) and for Q_{SH} is 1.01 W m^{-2} (13%), both of which are well within the accuracy of the buoy fluxes estimated by Moyer and Weller (1997).

b. The three coastal buoys (CMO, SESMOOR, and ASREX) in the western North Atlantic

In addition to the lack of daily variability, the T_s estimates have large warm biases at the CMO and SESMOOR sites. The bias is attributed to the coarse resolution in the NCEP2 (1.875° × 1.875° grid) and ECMWF (1.125° × 1.125° grid) models, which is insufficient to resolve the sharp thermal gradient surrounding the two buoy sites. As the region features frequent cyclonic storms in wintertime that usually last 2–3 days and have extremely high variability of $T_s - T_a$ and $q_s - q_a$, these two types of errors in T_s affect the Q_{LH} and Q_{SH} estimation considerably. The warm bias in T_s enhances $T_s - T_a$ and amplifies the sensible heat loss; it causes a wet bias in q_s, which contributes to the larger $q_s - q_a$ and the stronger latent heat loss. The mean overestimation bias for Q_{LH} is 15.9 W m^{-2} (20%) and for Q_{SH} is 10.5 W m^{-2} (34%) when averaged over the three buoys. The AVHRR observations have limited in-

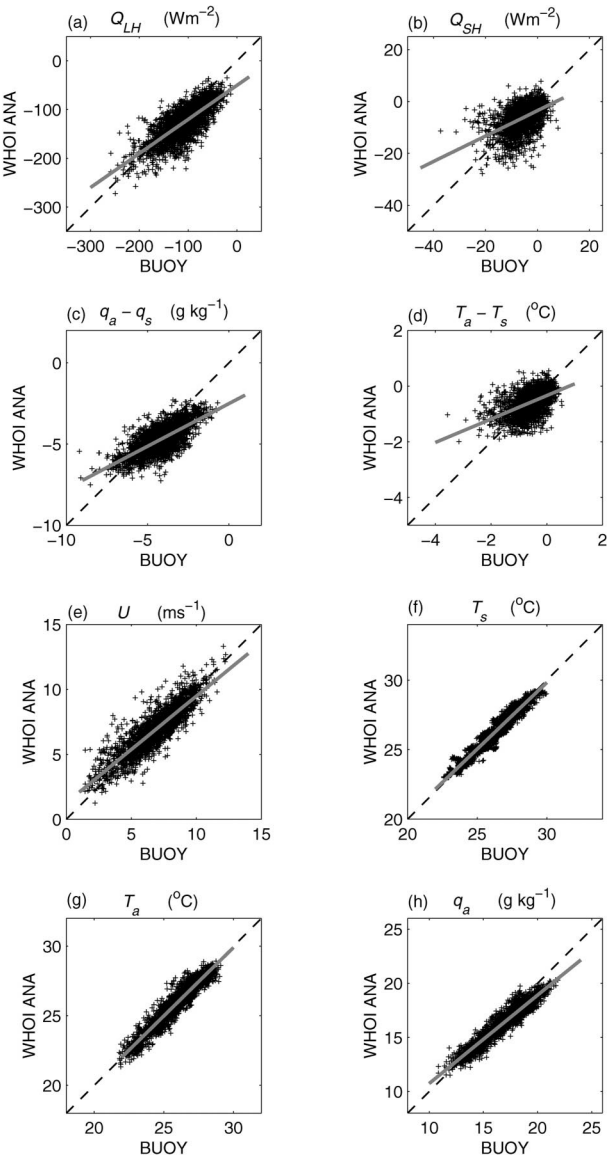

FIG. 11. As in Fig. 5 but constituted at the 11 buoy sites of the PIRATA experiment.

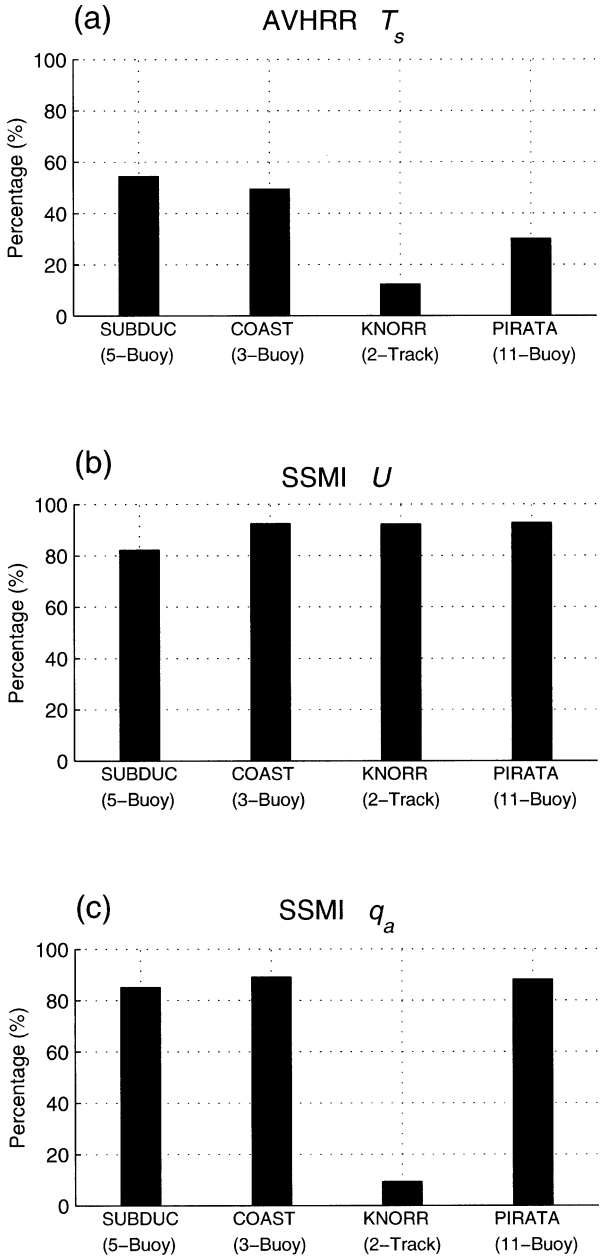

FIG. 12. Percentage of the number of days of available satellite observations relative to in situ measurement periods for the four experiment regions. (a) AVHRR, (b) SSM/I wind speed, and (c) SSM/I air humidity.

fluence on the T_s estimation because the cloudy skies associated with the stormy events affect the T_s retrieval from the AVHRR measurements.

c. *The two* Knorr *winter cruises in the Labrador Sea*

The T_s estimates are biased cold due to insufficient AHVRR observations and the crude representation of the sea ice mask in the ECMWF and NCEP2 models. But the errors in the $Q_{\rm LH}$ and $Q_{\rm SH}$ estimates do not directly reflect the errors in the T_s estimates because of the effect of error compensation. The cold biased T_s is the main cause for the dry biased $q_s - q_a$ and the underestimation bias in $Q_{\rm LH}$, while it is not the direct cause for the overestimation bias in $Q_{\rm SH}$. The latter is due to the error combination between cold biased T_s, cold biased T_a, and strong biased U. Along the two cruise tracks, the mean error for $Q_{\rm LH}$ is 8.7 W m^{-2} (7%) and for $Q_{\rm SH}$ is 9.7 W m^{-2} (6%).

d. *The 11 PIRATA buoys in the tropical Atlantic*

Similar to the Subduction Experiment site, the T_s estimates replicate well the seasonal trend but not the day-to-day variations. As the winds are mild and the mag-

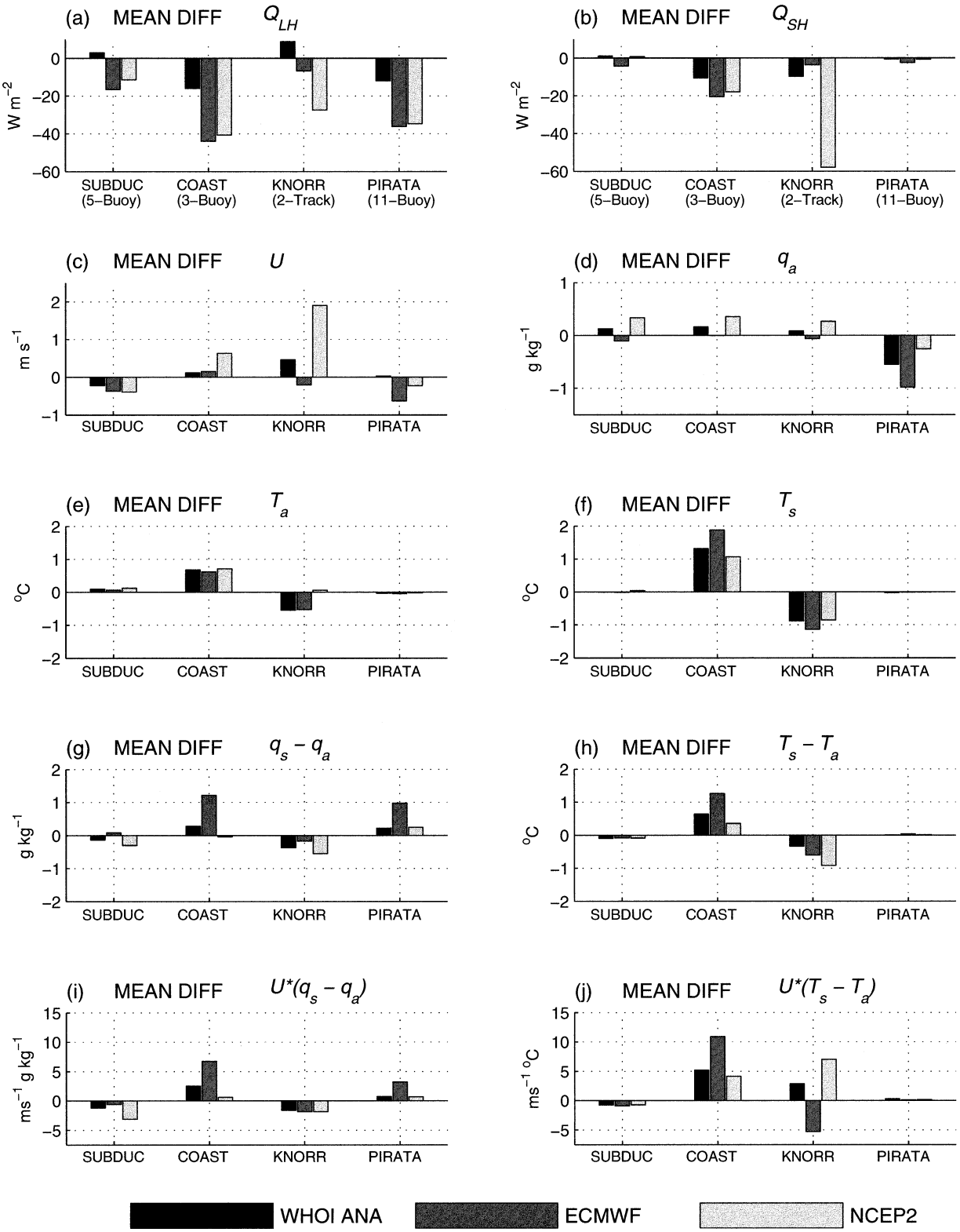

FIG. 13. Mean daily differences between the measurements and the WHOI analysis/ECMWF/NCEP2 averaged over the measurement periods: (a) Q_{LH}; (b) Q_{SH}; (c) U; (d) q_a; (e) T_a; (f) T_s; (g) $q_s - q_a$; (h) $T_s - T_a$; (i) $U(q_s - q_a)$; and (j) $U(T_s - T_a)$.

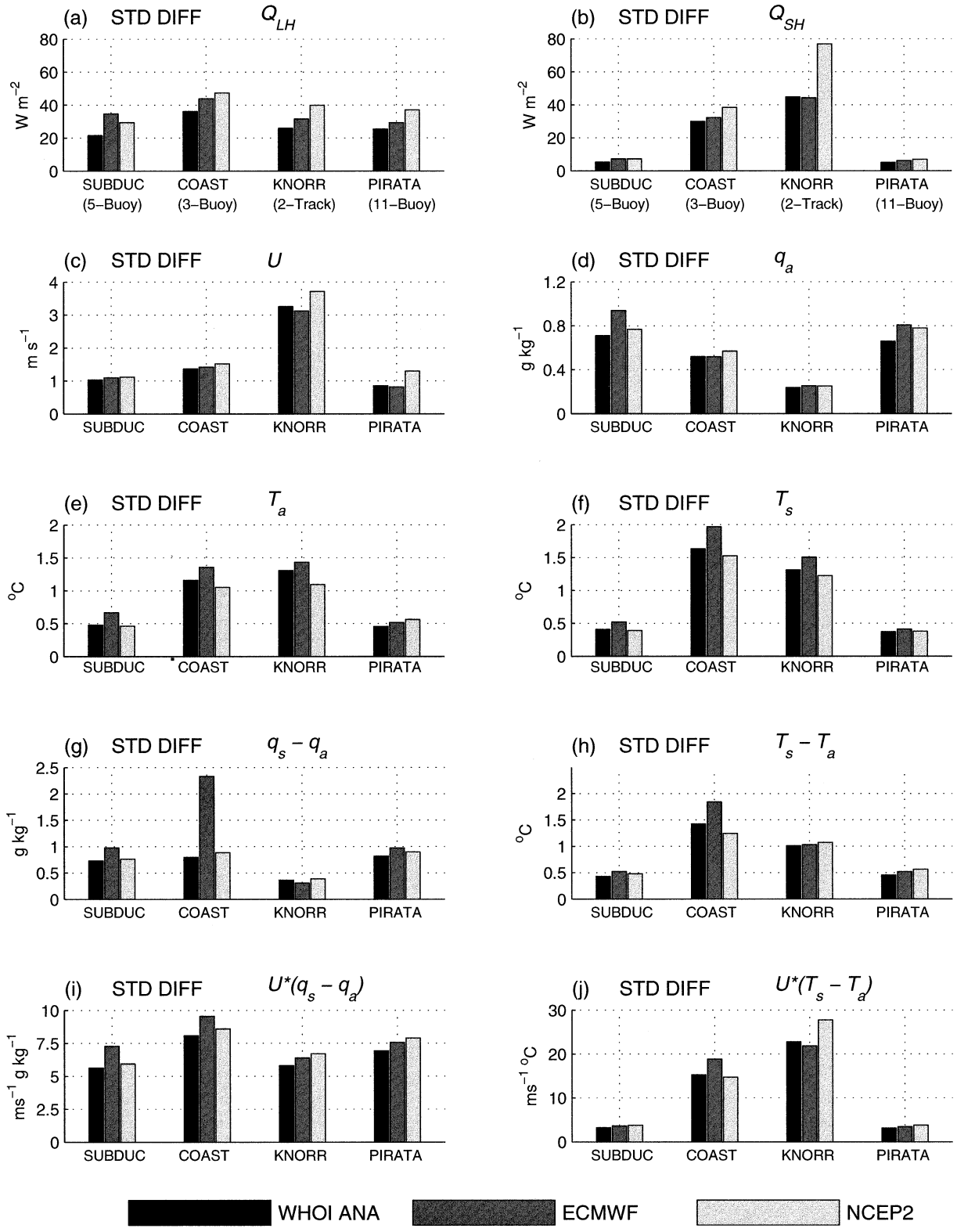

FIG. 14. As in Fig. 13 but for the standard deviation of the daily differences.

nitude of $T_s - T_a$ is small, the mean value of Q_{SH} is small (5.5 W m^{-2}), accounting for only 5% of the mean Q_{LH}. Both fluxes are overestimated, by 0.71 W m^{-2} (13%) for Q_{SH} and 11.9 W m^{-2} (11%) for Q_{LH}. Compared to the Q_{LH} estimates at the Subduction Experiment site, the larger bias in Q_{LH} is induced primarily by the dry biased q_a. Both ECMWF and NCEP2 model outputs and the q_a observations derived from SSM/I have a dry biased q_a, and this affects the WHOI q_a estimation.

Overall, the mean and daily variability of the latent and sensible heat fluxes from the WHOI analysis represent an improvement over the ECMWF and NCEP2 fluxes at all the measurement sites. Aside from the use of a better flux algorithm, basic variable estimates were improved by the WHOI analysis. The improvement in T_s and T_a was, however, relatively small due to insufficient satellite observations and larger biases in the ECMWF and NCEP2 outputs. Further improvement in the accuracy of latent and sensible heat fluxes will depend on the availability of high-quality SST observations. Better air humidity observations and/or improved representation by the ECMWF and NCEP models are also desired to further improve the accuracy of latent heat flux in the tropical Atlantic.

Acknowledgments. This work is supported by the NOAA CLIVAR-Atlantic program under Grant NA06GP0453. Simon Josey is thanked for his generosity in providing the monthly SOC data. The Data Support Section at NCAR is acknowledged for providing the ECMWF and NCEP data. The Subduction Experiment mooring array, CMO, SESMOOR, and ASREX moorings were deployed by the Upper Ocean Processes Group at WHOI; and the versions of the data from these experiments were prepared by N. Galbraith and A. Plueddemann. The PIRATA measurements were provided by the Tropical Atmosphere Ocean Project Office of the Pacific Marine Environmental Laboratory. The *Knorr* ship observations were kindly provided by Peter Guest. SSM/I wind speed data were downloaded from the Web site of Remote Sensing Systems (online at http://www.ssmi.com). AVHRR data were provided by JPL PODAAC and the SSM/I humidity retrievals by Shu-Hsien Chou. Barbara Gaffron read and edited the manuscript. A. Plueddemann and two anonymous reviewers are sincerely thanked.

REFERENCES

Bane, J. M., and K. E. Osgood, 1989: Winter-time air–sea interaction processes across the Gulf Stream. *J. Geophys. Res.*, **94,** 10 755–10 772.

Bolton, D., 1980: The computation of equivalent potential temperature. *Mon. Wea. Rev.,* **108,** 1046–1053.

Bradley, E. F., C. W. Fairall, J. E. Hare, and A. A. Grachev, 2000: An old and improved bulk algorithm for air–sea fluxes: COARE 2.6a. Preprints, *14th Symp. on Boundary Layers and Turbulence,* Aspen, CO, Amer. Meteor. Soc., 294–296.

Brown, J. W., O. B. Brown, and R. H. Evans, 1993: Calibration of AVHRR infared channels: A new approach to non-linear correction. *J. Geophys. Res.,* **98,** 18 257–18 268.

Brunke, M. A., C. W. Fairall, X. Zeng, L. Eymard, and J. A. Curry, 2003: Which bulk aerodynamic algorithms are least problematic in computing ocean surface turbulent fluxes? *J. Climate,* **16,** 619–635.

Bumke, K., U. Karger, and K. Uhlig, 2002: Measurements of turbulent fluxes of momentum and sensible heat over the Labrador Sea. *J. Phys. Oceanogr.,* **32,** 401–410.

Chou, S.-H., C.-L. Shie, R. M. Atlas, and J. Ardizzone, 1997: Air–sea fluxes retrived from Special Sensor Microwave Imager data. *J. Geophys. Res.,* **102,** 12 705–12 726.

——, E. J. Nelkin, J. Ardizzone, R. M. Atlas, and C.-L. Shie, 2003: Surface turbulent heat and momentum fluxes over global oceans based on the Goddard satellite retrievals, version 2 (GSSTFs). *J. Climate,* **16,** 3256–3273.

Crescenti, G. H., and R. A. Weller, 1992: Analysis of surface fluxes in the marine boundary layer in the vicinity of rapidly intensifying cyclones. *J. Appl. Meteor.,* **31,** 831–848.

——, S. A. Tarbell, and R. A. Weller, 1991: A compilation of moored current meter data and wind recorder data from the Severe Environment Surface Mooring (SESMOOR). Woods Hole Oceanographic Institute Tech. Rep. WHOI-91-18, Woods Hole, MA, 59 pp.

Daley, R., 1991: *Atmospheric Data Analysis.* Cambridge University Press, 457 pp.

ECMWF, 1994: The description of the ECMWF/WCRP levels III–A atmospheric data archive. ECMWF Tech. Attachment, 72 pp.

Fairall, C. W., E. F. Bradley, D. P. Rogers, J. B. Edson, and G. S. Young, 1996: Bulk parameterization of air–sea fluxes for TOGA COARE. *J. Geophys. Res.,* **101,** 3747–3764.

Galbraith, N. R., A. Gnanadesikan, W. M. Ostrom, E. A. Terray, B. S. Way, N. J. Williams, S. H. Hill, and E. Terrill, 1996: Meteorological and oceanographic data during the ASREX III field experiment: Cruise and data report. Woods Hole Oceanographic Institute Tech. Rep 96-10, Woods Hole, MA, 247 pp.

——, A. Plueddemann, S. Lentz, S. Anderson, M. Baumgartner, and J. Edson, 1999: Coastal mixing and optics experiment moored array data report. Woods Hole Oceanographic Institute Tech. Rep. WHOI-99-15, Woods Hole, MA, 162 pp.

Gleckler, P. J., and B. C. Weare, 1997: Uncertainties in global ocean surface heat flux climatologies derived from ship observations. *J. Climate,* **10,** 2764–2781.

Josey, S. A., 2001: A comparison of ECMWF, NCEP–NCAR, and SOC surface heat fluxes with moored buoy measurements in the subduction region of the northeast Atlantic. *J. Climate,* **14,** 1780–1789.

——, E. C. Kent, and P. K. Taylor, 1998: The Southampton Oceanography Centre (SOC) ocean–atmosphere heat, momentum and freshwater flux atlas. Southampton Oceanography Centre, Rep. 6, Southampton, United Kingdom, 30 pp. + figs.

——, ——, and ——, 1999: New insights into the ocean heat budget closure problem from analysis of the SOC air–sea flux climatology. *J. Climate,* **12,** 2856–2880.

Kalnay, E., and Coauthors, 1996: The NCEP/NCAR 40-Year Reanalysis Project. *Bull. Amer. Meteor. Soc.,* **77,** 437–471.

Kanamitsu, M., 1989: Description of the NMC global data assimilation and forecast system. *Wea. Forecasting,* **4,** 334–342.

——, W. Ebisuzaki, J. Woolen, J. Potter, and M. Fiorion, 2000: An overview of NCEP/DOE reanalysis-2. *Proc. 2d Int. Conf. on Reanalyses,* Reading, England, WMO, 1–4.

Marshall, J., and Coauthors, 1998: The Labrador Sea Deep Convection Experiment. *Bull. Amer. Meteor. Soc.,* **79,** 2033–2058.

Moyer, K. A., and R. A. Weller, 1997: Observations of surface forcing from the Subduction Experiment: A comparison with global model products and climatological datasets. *J. Climate,* **10,** 2725–2742.

Renfrew, I. A., G. W. K. Moore, P. S. Guest, and K. Bumke, 2002: A comparison of surface layer and surface turbulent flux ob-

servations over the Labrador Sea with ECMWF analyses and NCEP reanalyses. *J. Phys. Oceanogr.*, **32,** 383–400.

Reynolds, R. W., and T. M. Smith, 1994: Improved global sea surface temperature analyses using optimum interpolation. *J. Climate,* **7,** 929–948.

Roebber, P. J., 1984: Statistical analysis and updated climatology of explosive cyclones. *Mon. Wea. Rev.*, **112,** 1577–1589.

Schulz, J., P. Schlüssel, and H. Graßl, 1993: Water vapor in the atmospheric boundary layer over oceans from SSM/I measurements. *Int. J. Remote Sens.*, **14,** 2773–2789.

Servain, J., A. J. Busalacchi, M. J. McPhaden, A. D. Moura, G. Reverdin, M. Vianna, and S. E. Zebiak, 1998: A Pilot Research Moored Array in the Tropical Atlantic (PIRATA). *Bull. Amer. Meteor. Soc.*, **79,** 2019–2031.

Smith, S. R., D. M. Legler, and K. V. Verzone, 2001: Quantifying uncertainties in NCEP reanalyses using high-quality research vessel observations. *J. Climate,* **14,** 4062–4072.

Sun, B., L. Yu, and R. A. Weller, 2003: Comparisons of surface meteorology and turbulent heat fluxes over the Atlantic: MWP model analyses versus moored buoy observations. *J. Climate,* **16,** 679–695.

Wang, W., and M. J. McPhaden, 2001: What is the mean seasonal cycle of surface heat flux in the equatorial Pacific? *J. Geophys. Res.*, **106,** 837–857.

Weller, R. A., and S. P. Anderson, 1996: Surface meteorology and air-sea fluxes in the western equatorial Pacific warm pool during the TOGA COARE. *J. Climate,* **9,** 1959–1990.

——, M. F. Baumgartner, S. A. Josey, A. S. Fisher, and J. C. Kindle, 1998: Atmospheric forcing in the Arabian Sea during 1994–1995 observations and comparisons with climatology models. *Deep-Sea Res.*, **45B,** 1961–1999.

Wentz, F. J., 1997: A well-calibrated ocean algorithm for SSM/I. *J. Geophys. Res.*, **102,** 8703–8718.

Yu, L., B. Sun, and R. A. Weller, 2002: Developing daily latent and sensible heat fluxes for the Atlantic Ocean by synthesizing satellite retrievals and outputs of numerical weather prediction models (1988–1999). WHOI Tech. Rep., 38 pp. + 14 figures.

——, R. A. Weller, and B. Sun, 2004: Improving latent and sensible heat flux estimates for the Atlantic Ocean (1988–99) by a synthesis approach. *J. Climate,* **17,** 373–393.

Zeng, X., M. Zhao, and R. E. Dickinson, 1998: Intercomparison of bulk aerodynamic algorithms for the computation of sea surface fluxes using the TOGA COARE and TAO data. *J. Climate,* **11,** 2628–2644.